Rev.Adv.Mater.Sci. 4 (2003) 79-113

DISCLINATIONS AND ROTATIONAL DEFORMATION IN NANOCRYSTALLINE MATERIALS

M.Yu. Gutkin and I.A. Ovid'ko

Institute of Problems of Mechanical Engineering, Russian Academy of Sciences, Bolshoj 61, Vas. Ostrov, St.Petersburg, Russia

Received: June 2, 2003

Abstract. Role of disclinations and rotational modes of plastic deformation in fine-grained materials is discussed. First, we consider disclination models of generation and development of misorientation bands in severely deformed metals and alloys. The models predict the existence of the critical external shear stress, above which nucleation of misorientation bands takes place. The further analysis demonstrates two main regimes of misorientation band development: stable and unstable propagation, and allows to find another critical stress that controls the transition between these two regimes. We quote also some results of computer simulations of 2D dynamics of dislocations in the stress field of a dipole of partial wedge disclinations to elucidate the micromechanisms of misorientation band propagation. Second, theoretical models of grain boundary disclination motion in fine-grained materials are considered. This motion leads to changes in misorientations across the grain boundaries and may explain the rotation of grain crystalline lattice as a whole. It is demonstrated that motion of grain boundary disclinations may occur in fine-grained materials through emission of pairs of lattice dislocations into the adjacent grains or through climb of grain boundary dislocations. We also consider a model of crossover from grain boundary sliding to rotational deformation which is realized by the transformation of a pile-up of gliding grain boundary dislocations stopped by a triple junction of grain boundaries, into two walls of climbing grain boundary dislocations (treated as the dipoles of partial wedge disclinations). The conditions necessary for such a transformation are determined and discussed.

INTRODUCTION

Appearance in the early 1980s of the first nanocrystalline materials (NCMs) [1, 2] has stimulated a great interest to disclinations as a powerfull mean to describe the structure and mechanical behavior of nano-objects. Geometric and elastic properties of wedge disclinations were applied to model the pentagonal symmetry and strained state in nanoparticles [3-11], to explain the abnormal Hall-Petch relation [12-17] and various grain-boundary phenomena [8, 9, 11, 13-27] in NCMs, to study possible ways of misfit-strain accommodation in heterogeneous nano-layered structures [28-38], etc.

The aforementioned applications were based on continual description of disclinations in the framework of the classical theory of elasticity which allows to obtain the solutions of various (sometimes quite complicated) boundary-value problems for elastic fields of disclinations localized in nano-volumes (e.g., see reviews [8, 39-41] and original papers [4, 6, 42-49]). However, some components of these fields are singular at the disclination lines, a fact that limits the applicability of the classical theory to consider situations where it is important to know the strained state near disclination lines. This concerns, for example, disclination models for grain boundaries and their triple junctions in NCMs where one deals with high-density ensembles of disclinations.

To avoid this problem, in recent years much effort has been spent to describe both the wedge and twist disclinations within non-classical theories such as the nonlocal theory of elasticity [50, 51], gradient theory of elasticity [52-55] and gauge theory of elastoplasticity [56, 57], all of which allow to dispense with the classical singularities. By using the

Corresponding author: M.Yu. Gutkin, e-mail: gutkin@def.ipme.ru

gradient solutions, the short-range elastic interactions between disclinations in an infinite solid were studied [52, 55], while the gauge solution gave non-singular elastic fields for a wedge disclination placed along the axis of a thin cylinder [56]. It is worth noting that the non-classical solutions obtained within these quite different theories, totally coincide. Nevertheless, application of these new results to the theory of mechanical behavior of NCMs is still an open question.

Extensive investigations of structure, properties and fabrication methods of NCMs which have been carried out during last two decades (e.g., see reviews [1, 2, 9, 16, 17, 58-75], monographs [27, 76-80] and collections of papers [81-93]), have shown that NCMs qualitatively differ from conventional polycrystals. First, this concerns the structure of grain (intercrystalline) boundaries whose thickness in NCMs may achieve 1-2 nm. It means that the grain boundaries (GBs) themselves are typical nano-objects – the layers of material which often has the other atomic structure and sometimes is much more porous than the material inside the grains (crystallites). Comparison of different experimental data from Mössbauer spectroscopy [94], positron lifetime spectroscopy [95, 96], X-ray diffraction [97], EXAFS [98], neutron diffraction [99] and HREM [100] allowed to conclude that a significant part of the GBs in NCMs have severely distorted near-boundary regions with smaller atomic density and higher level of elastic strains [100]. For example, microstructure studies [100] of nanocrystalline palladium with the grain size of 4-9 nm, which was fabricated by high-pressure-compaction of nanocrystallites condensed from the gas phase, demonstrated that it contains $\approx$ 40 vol. % of undistorted crystalline material, $\approx$ 25% of stretched or amorphous-type GB layers, $\approx$ 25% of highly strained material, and $\approx$ 10% of pores. Inside the grains, they observed lamellae of twins, low-angle boundaries and dislocations localized near the GBs. Under thermal annealing, this system was transformed into a conventional polycrystalline structure with thin GBs and undistorted grains.

Besides the GBs, their triple junctions play an important role in the behavior of NCMs. Indeed, if the mean grain size is of some nanometers and the GB thickness equals 1-2 nm, then the volume fraction of the triple junction material is very high (up to 50 % and even more) in such NCMs. In recent years, it has been definitely recognized that triple junctions of GBs have the structure and properties being different from those of the GBs that they adjoin [101]. From experimental data and theoretical models [18-20, 101-108] it follows that the triple junctions act as enhanced diffusivity tubes, nuclei of the second phase segregation, strengthening elements and sources of lattice dislocations during plastic deformation, and drag centers of GB migration during re-crystallization processes. In particular, the outstanding diffusional properties exhibited by NCMs [79, 109-112] are viewed to be related to the effect of the highly enhanced diffusion along triple junction tubes [2].

These key features of NCMs (i.e., high density of GBs and GB triple junctions with their generic defects like GB dislocations and disclinations) which mainly determine their mechanical properties, may stimulate, under special conditions, the generation and development of rotational mode of plastic flow. This mainly concerns the NCMs fabricated under highly non-equilibrium conditions like ball milling and severe plastic deformation. In the present review we consider different models of rotational plastic deformation in nano- and polycrystalline materials. In the first part of the paper we discuss disclination models for misorientation bands in severely deformed metals and alloys. The models predict the existence of the critical external shear stress, above which nucleation of misorientation bands takes place. The further analysis demonstrates two main regimes of misorientation band development: stable and unstable propagation, and allows to find another critical stress that controls the transition between these two regimes. We quote also some results of computer simulations of 2D dynamics of dislocations in the stress field of a dipole of partial wedge disclinations to elucidate the micromechanisms of misorientation band propagation. The second part of the paper is devoted to the theoretical models of GB disclination motion which leads to changes in misorientations across the GBs in NCMs and may explain the rotation of nanograin crystalline lattice as a whole. It is demonstrated that motion of GB disclinations may occur in NCMs through emission of pairs of lattice dislocations into the adjacent grains or through climb of GB dislocations. We consider a model of crossover from GB sliding to rotational deformation which is realized by the transformation of a pile-up of gliding GB dislocations stopped by a triple junction of GBs, into two walls of climbing GB dislocations (treated as the dipoles of partial wedge disclinations). The conditions necessary for such a transformation are determined and discussed.

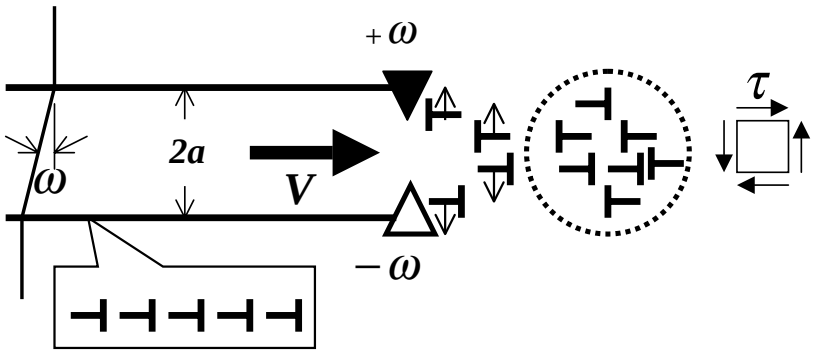

Fig. 1. Dislocation-disclination model of a misorientation band propagation with the velocity $\vec{V}$ under the action of external shear stress τ. The front of the misorientation band is modelled as a two-axes dipole of partial wedge disclinations of strength ±ω.

2. GENERATION AND DEVELOPMENT OF MISORIENTATION BANDS

During the two last decades, the concept of disclinations has been broadly applied to treat mesoscopic substructures which are characteristic for metals and alloys under large deformation (e. g., see [8, 113-116] for a review). Misorientation bands (MBs) represent one of the typical elements of such substructures. They are observed as long straight strips of material having a crystallographic orientation different from that of neighbouring areas of the material [8, 113, 115-125]. The boundaries of such MBs (i.e., the misorientation boundaries) are often illustrated as low-angle dislocation tilt boundaries, although they have a finite thickness of about 0.1-0.5 μm depending on the deformation magnitude [113], and consist in fact of high-density dislocation arrangements. Works [123, 124] give a review of experimental data on MBs and other different rotational structures in various high-strength materials including submicrocrystalline metals and alloys. Based on these results as well as on recent direct atomic-level observations of dipoles of partial disclinations in mechanically milled, nanocrystalline iron [126], one can assume the possibility of MB generation in typical NCMs under large deformation.

The appearance and development of MBs represents one of the ways of rotational plastic flow in heavily deformed metals. MBs were found at the beginning of the 1960s in TEM experiments [117, 118] (see also [8, 114] for a review). In the 1970s and 1980s, they were extensively studied and directly connected with the formation of specific dislocation structures which may be described through partial disclinations (see [8, 113-116] and references therein). Indeed, the presence of two edges of the misorientation boundaries which border the MB area, allows to introduce a corresponding dipole of partial disclinations whose strength is equal to the misorientation angle characterizing the MB [127]. In Fig. 1, the edges of the tilt misorientation boundaries are shown as a two-axes dipole of partial wedge disclinations of strength ω. Such a disclination dipole is geometrically related to the MB parameters through the equation [8], $b\rho = b/l = 2\tan(\omega/2)$, for a dislocation tilt boundary. Here b denotes the Burgers vector magnitude of the dislocations composing the boundary, ρ is their linear density along the boundary, l is the interdislocation spacing, and ω is the angle of misorientation across the boundary. In the case of small misorientation angles, $\omega << 1$, this relationship is transformed into $\rho = 1/l = \omega/b$. Also, the width of the MB is equal to the arm $2a$ of the disclination dipole (Fig. 1).

In 1978, Vladimirov and Romanov [127] proposed a dislocation-disclination model to describe the mechanism of MB propagation. The main idea of the model is that the elastic stresses created by the disclination dipole (Fig. 1), divide a statistically arranged dislocation ensemble in front of the MB into groups of “positive” and “negative” dislocations. The terms, “positive” or “negative”, are caught by the positive or negative disclinations, respectively. Every event of capturing of a dislocation dipole by the disclination dipole leads to an elementary act of the MB conservative motion. The mechanism [127] has been experimentally approved [8, 113] and used in modeling the dislocation-disclination kinetics in metals under large deformation [8, 114-116, 128-

131]. However, there is a number of questions which are still open. In particular, details of dislocation capture by disclination dipoles are still unknown. Moreover, computer simulations of elastic interactions between partial disclinations and edge dislocations [132] (see also Section 2.4 of the present paper) have shown that the simple scheme (Fig. 1) proposed in [127], can not provide complete description of MB propagation and has to be elucidated further.

Generally speaking, the partial disclinations which are used in describing MBs, are associated by definition with terminated misorientation boundaries in otherwise perfect crystals [8]. The nature of such boundaries as well as their atomic structure may be quite different. They can be low angle dislocation walls, high angle grain boundaries or twin boundaries. Anyway, the boundary edges may be described (both geometrically and elastically) as the lines of partial disclinations of corresponding strength. Therefore, the long-range elastic fields (far from the misorientation boundaries themselves) of displacement, strain and stress of a terminated misorientation boundary may be calculated with the help of well-developmed mathematics of wedge disclinations within the classical [8, 133] or nonclassical [50-56] theories of elasticity.

It is well documented [8, 113-116, 119, 123, 124] that possible sites for MB generation in polycrystalline metals are various faults (defects) of GBs including kinks, double and triple junctions of GBs. In nanocrystalline solids, such GB faults often contain disclinations, even in an initial as-sintered state [8, 9, 11-27, 126]. However, nowadays there is only one theoretical work [125] containing the models that allows to describe the MB generation and predicts appropriate critical conditions as well as regimes of MB propagation. The well-known dislocation-disclination model of MB propagation by Vladimirov and Romanov [127] represents mainly geometrical features and needs further development.

In paper [125] the models of initial disclination configurations at GB kinks and junctions were proposed. It was shown these initial configurations may serve as sources for MB generation when the applied shear stress achieves a critical value. Further development of the generated MB may be stable or unstable, depending on the level of applied shear stress. If this level is lower than another critical value, the stable regime of MB propagation is realized, if higher – unstable. For the case of stable propagation, an equilibrium length of the MB was introduced and studied. All of these results were obtained in the framework of a quasiequilibrium thermodynamic approach when only the necessary (not sufficient) conditions for MB generation and propagation were analyzed [125]. To obtain the sufficient conditions, one should investigate the dynamics of these processes which must be based on the dynamics of complicated dislocation structures, first, at the place of MB nucleation, and second, in front of the propagating MB. In a general three-dimensional (3D) case this problem is very hard. However, in a 2D model case, when the lines of all dislocations and partial disclinations are assumed to be straight and parallel to each other, it can be solved by means of computer simulation within coupled dislocation-disclination dynamics [125, 132]. It is worth noting that computer simulation and modeling of discrete dislocation ensembles represent nowadays one of the most popular topics in theoretical materials science. Since the late 1980s, 2D and 3D calculations of the dynamics of interacting dislocations have intensively been developed (e.g., see reviews [134, 135] and some recent papers on 2D [136, 137] and 3D [138, 139] mesoscopic simulations). However, no other attempts but [125, 132] have been known to the authors, which would be aimed at a correct simulation of dislocation-disclination ensembles. The former computer models [114, 128-131] describing the coupled evolutional kinetics of dislocations and partial disclinations practically did not take into account the elastic interactions between them. In contrast, papers [125, 132] contain the first results of 2D computer simulation of the coupled dynamics of partial disclnation dipoles and edge dislocations aimed at studying peculiarities of elastic interaction between these defects. These results were assumed to be used further for checking and refining the existing theoretical (non-computer) models of MB development. In the following Sections we will consider the models presented in [125, 132] in more detail.

2.1. Initial disclination configurations at grain boundary junctions

Consider a simple scenario [125], shown schematically in Fig. 2, which may be applied to initial disclination configuration formation at a GB. Let some gliding dislocations with Burgers vectors $\vec{b}_1$ cross a flat GB (Fig. 2a) and move into the neighbouring grain where the gliding dislocations have Burgers vectors $\vec{b}_2$ (Fig.2b). As a result, a wall of difference dislocations having Burgers vectors $\delta\vec{b} = \vec{b}_1 - \vec{b}_2$ and interdislocation spacing l, appears at the crossing site together with the GB kink. On a mesoscale level, when the characteristic scale of

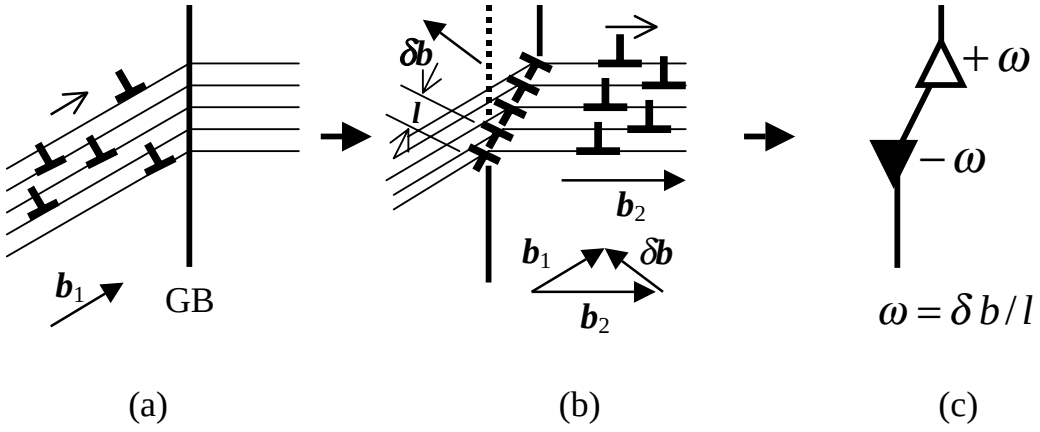

Fig. 2. A simple model of the formation of an initial grain boundary disclination dipole with the strength ω.

consideration *L* is much larger than *l*, the geometry and resulting elastic fields for such a difference dislocation wall may be effectively described as those of a two-axes dipole of wedge partial disclinations with strengths $\pm\omega = \pm\delta b/l$ [8, 133] (Fig.2c).

Such a simple scheme of GB disclination dipole formation is possible to occur in NCMs with relatively large grains which are capable to deform by usual glide of lattice dislocations. This may concern, for example, both the micro- and nanocrystalline metals and alloys fabricated by intensive plastic deformation [23, 25, 27, 126, 140]. In a real conventional polycrystalline material, the initial disclination configurations at GBs result from more complicated processes which are typical for the stage when translational deformation modes are replaced by rotational ones [8, 113]. It is well established [113] that in the vicinity of GB kinks or junctions, the dislocation cells have smaller size than far from such sites as is illustrated schematically in Fig.3a [125]. This means that within these areas, the density of GB difference dislocations must be much higher than at straight or smooth segments of GBs. As a corollary, one can assume the formation of initial quadrupole-like disclination configurations at GB kinks or junctions. In Fig. 3b, three possible quadrupole-like disclination configurations are shown where α, β, ω and θ denote the disclination strengths. For simplicity, to catch mostly qualitative features and make rough estimates, the authors [125] considered only wedge partial disclinations. It is worth noting that the sum strength of any such disclination configuration must be equal to zero or, in other words, the sum strength of positive disclinations must be equal to that of negative disclinations within a GB disclination configuration (Fig.3b).

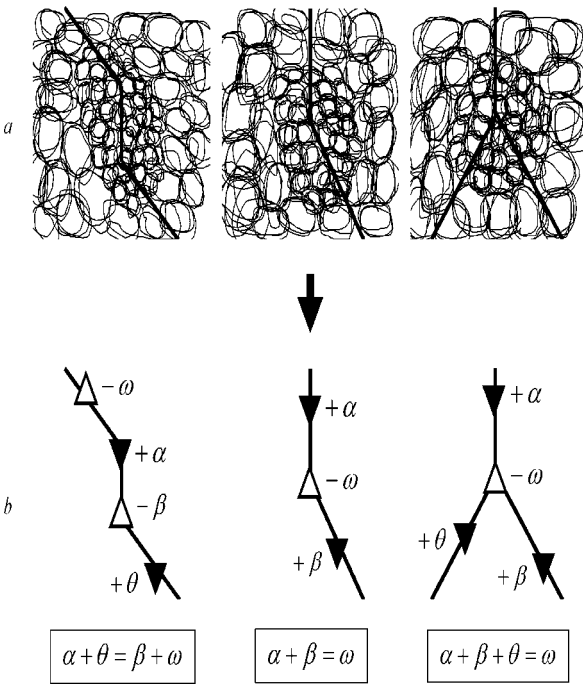

Fig. 3. More realistic models of the formation of initial grain boundary quadrupole-like disclination configurations.

2.2. Generation of misorientation bands

2.2.1. Splitting of an initial GB disclination dipole

Consider the simplest initial GB disclination configuration that is a GB disclination dipole (Fig.4a) [125]. Let this dipole be under an external shear stress τ. It is also assumed that around the dipole is typical dislocation-cell structure. Under the action of the internal shear stress (which is caused by

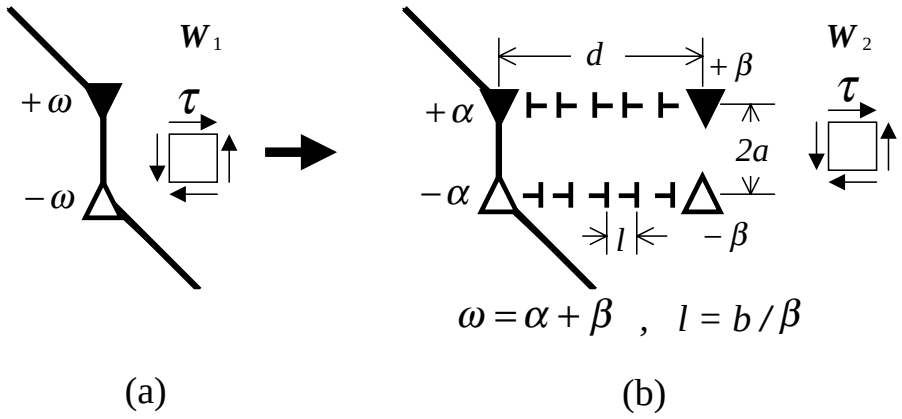

Fig. 4. Generation of a misorientation band by splitting of an initial grain boundary disclination dipole.

the GB disclination dipole) and external shear stress τ, the dislocations from the cell boundaries nearest to the disclinations have to glide to them thus forming two dislocation walls, i.e., a new disclination configuration (Fig.4b) [125]. The latter may be considered as produced by splitting of the initial GB disclination dipole. This new split configuration is characterized by the split distance d, the interdislocation spacing l, the dipole arm $2a$ and the disclination strengths $\pm\alpha$ and $\pm\beta$ satisfying the relationships $\beta = b/l$ and $\omega = \alpha + \beta$, where b is the module of Burgers vector for lattice dislocations and ω is the initial strength of the dipole. In fact, the new split disclination configuration represents a model for a MB of finite length which consists of a new immobile GB disclination dipole having the strength α (α-dipole), a new mobile disclination dipole with the strength β (β-dipole), and two misorientation boundaries of the length d.

To make possible the transition from the initial GB disclination dipole to the new split configuration, the total energy of the initial dipole must be larger than that of the new split configuration. Thus, to find critical conditions for such a transition, one has to calculate and compare these energies.

The total energy of the initial GB disclination dipole may be calculated as the work necessary to generate this dipole in its proper elastic stress field [8]. As a result, the energy per unit length of disclinations reads

$$W_1 = D\omega^2 a^2 \left(2\ln\frac{R}{2a} + 1 \right), \qquad (1)$$

where $D=G/[2\pi(1-\nu)]$, G is the shear modulus, ν is the Poisson ratio, and R is a characteristic parameter of screening of the disclination long-range elastic fields (e.g., the size of a sample).

The total energy of the new split configuration (per unit length of disclinations) was written in [125] as the following sum

$$W_2 = W_\alpha + W_\beta + W_{\alpha-\beta} + 2\gamma d - A, \qquad (2)$$

where W_α and W_β are the elastic energies of α- and β-dipoles (Fig.4b), respectively, $W_{\alpha-\beta}$ is the energy of their interaction, γ the effective surface energy of the two new misorientation boundaries, and A the work by the external shear stress τ on the displacement d of the mobile β-dipole. The terms W_α and W_β are similar to that given by Eq. 1 with the replacement of ω by α and β, respectively. The energy of the dipole-dipole interaction $W_{\alpha-\beta}$ was calculated as the work during the generation of one dipole in the stress field of another dipole, thus resulting in [125]

$$W_{\alpha-\beta} = 2D\alpha\beta a^2 \left(\ln\frac{R^2}{4a^2+d^2} - \frac{d^2}{4a^2}\ln\frac{4a^2+d^2}{d^2} + 1 \right). \qquad (3)$$

The work A was found in a similar way that gave $A=2\tau\beta ad$.

To estimate γ, the authors [125] used the well-known approximation for the energy of a dislocation core [141] $W_c \approx Db^2/2$. Due to geometric reasons [141], the linear density of "geometrically-necessary" dislocations [142] ρ_g within a misorientation boundary is equal to β/b. However, it was necessary also to take into account the density of "statistically-stored" dislocations [142] which have different orientations of their Burgers vectors and do not create

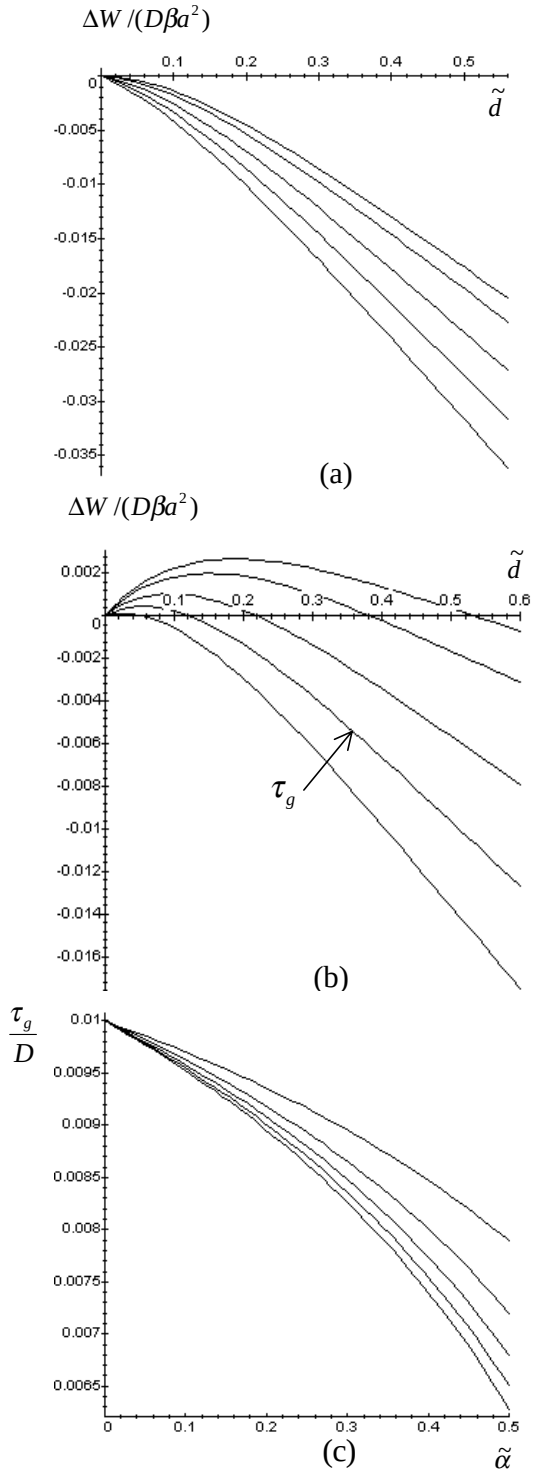

Fig. 5. Energy difference ΔW via the normalized misorientation band length $\tilde{d}$ (a, b) and critical shear stress τ_g/D via the normalized grain boundary disclination dipole strength $\tilde{\alpha}$ (c) for the model of a misorientation band being generated at a grain boundary disclination dipole. The plots $\Delta W(\tilde{d})$ are given for the external shear stress τ/D=0, 0.001, 0.003, 0.005, and 0.007 (from top to bottom) for the two different values of the parameter q=1 (a) and 10 (b). The plots $\tau_g(\tilde{\alpha})/D$ are shown for the initial dipole strength ω =0.01, 0.02, 0.03, 0.04, and 0.05 (from top to bottom).

any additional misorientation but give their income into the effective surface energy of the boundary. Let the total dislocation density within the misorientation boundaries $\rho_t = q\rho_g$, where $q \geq 1$ is a dimensionless parameter which accounts the presence of "statistically-stored" dislocations. Hence, the number of dislocation cores, N, within a misorientation boundary is estimated as $N = \rho_t d = q\beta d/b$ and the total core energy of a misorientation boundary is $NW_c \approx qD\beta bd/2$. Thus, the approximation $\gamma \approx NW_c/d \approx qD\beta b/2$ was found [125].

Let us consider now the energy difference [125]

$$\Delta W = W_2 - W_1 = D\beta a^2 \left\{ 4\tilde{d}\left(q\tilde{b} - \frac{\tau}{D} \right) - 2\alpha\left[(1+\tilde{d}^2)\ln(1+\tilde{d}^2) - \tilde{d}^2 \ln \tilde{d}^2 \right] \right\}, \quad (4)$$

where the dimensionless quantities $\tilde{d} = d/2a$ and $\tilde{b} = b/2a$ were introduced. The dependence of ΔW on the normalized displacement $\tilde{d}$ is given in Fig. 5 for $\tilde{b} = 10^{-3}$, $\alpha = \pi/200$, and different values of the external shear stress τ and parameter q [125]. Depending on τ and q, the character of the curves $\Delta W(\tilde{d})$ changes drastically from monotonous decreasing (Fig. 5a) to non-monotonous one (Fig. 5b). In the first case, when q=1 while τ and d are small enough (here $0 \leq \tau \leq 0.007D$ and $\tilde{d} < 1$), $\Delta W < 0$ for $\tilde{d} > 0$. This means there is no energy barrier for the generation of a MB. In the second case, when q=10 with the same values of τ and $\tilde{d}$, $\Delta W > 0$ for $\tilde{d} < \tilde{d}_c$, where $\tilde{d}_c$ is determined by the equation $\Delta W(\tilde{d} = \tilde{d}_c) = 0$, and $\Delta W < 0$ for $\tilde{d} > \tilde{d}_c$. This means there is an energy barrier for the formation of a MB under such a small τ. Following [125], let us introduce a characteristic critical value τ_g which is determined by the equation $\tilde{d}_c = \tilde{l}$, where $\tilde{l} = l/2a$ is the normalized spacing between the "geometrically-necessary" dislocations creating the tilt misorientation angle β. If $\tau < \tau_g$, the generation of a MB nucleus (an initial GB disclination dipole plus one dislocation dipole joined to this dipole and localized at the distance $\tilde{l}$ from it) is energetically unfavourable; if $\tau > \tau_g$, it is favourable. For the situation illustrated in Fig.5b, $\tilde{l} \approx 0.1$ was assumed and hence $\tau_g \approx 0.005D$ for q=10.

Using Eq. 4, one can analytically estimate τ_g for the case $\tilde{d} \ll 1$ as follows [125]

$$\tau_g \approx D\tilde{b}\left\{ q - \frac{\tilde{\alpha}}{1-\tilde{\alpha}}\left(\frac{1}{2} - \ln \frac{\tilde{b}/\omega}{1-\tilde{\alpha}} \right) \right\}, \quad (5)$$

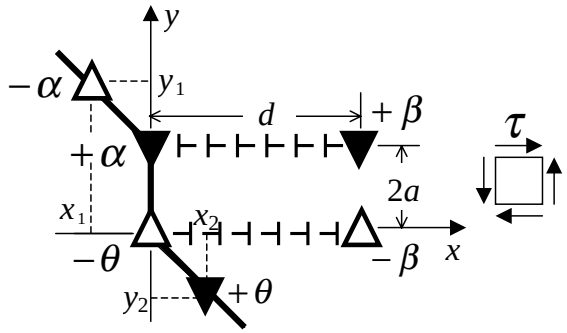

Fig. 6. Model of misorientation band generation by splitting of an initial quadrupole-like disclination configuration at a grain boundary kink.

where $\tilde{\alpha}=\alpha/\omega$. The plots $\tau_g(\tilde{\alpha})$ are shown in Fig.5c for q=10 and various values of the initial dipole strength ω [125]. One can conclude that τ_g decreases when both $\tilde{\alpha}$ and ω increase that is in accordance with physical intuition. When q=10, the numerical estimate for τ_g gives the values of order G/1000-G/400. The lower limit fits well with typical external stresses at the end of Stage II of deformation curves for BCC and FCC metals [113], while the upper limit corresponds to the level of deforming stress observed in NCMs [16, 17, 78].

2.2.2. Splitting of an initial quadrupole-like disclination structure at a GB kink

Consider now a model which seems to be more realistic than the previous one. It is a GB kink with a quadrupole-like disclination structure (Fig.6) [125]. This configuration is characterized by the disclination strengths -α, +γ, -ω and +θ which satisfy the equation: $\alpha + \omega = \gamma + \theta$. As a result of the dislocation rearrangements which are suggested similar to those considered above, the quadrupole-like disclination structure issues a mobile two-axes dipole of partial wedge disclinations having the strengths $\pm\beta$ and moving under the action of the GB disclination stress field as well as an external shear stress τ (Fig. 6) [125]. In a special simple case, the new split configuration was suggested to consist of three two-axes disclination dipoles, one mobile (β-dipole) and two immobile (α- and θ-dipole). Again, to find critical conditions for such a splitting transformation, the total energy, W_1, of the initial quadrupole-like disclination structure and that, W_2, of the new split configuration were compared.

The energy difference $\Delta W=W_2-W_1$ was calculated as shown above and resulted in [125]

$$\Delta W = D\beta a^2\left\{4\tilde{d}\left(q\tilde{b}-\frac{\tau}{D}\right)-(\alpha+\theta)\left[(1+\tilde{d}^2)\ln(1+\tilde{d}^2)-\tilde{d}^2\ln\tilde{d}^2\right]+\alpha\Psi(\tilde{x}_1,\tilde{y}_1,\tilde{d})-\theta\Psi(\tilde{x}_2,\tilde{y}_2,\tilde{d})\right\}, \quad (6)$$

where

$$\Psi(x,y,z) = -(x^2+y^2)\ln(x^2+y^2)+\left[x^2+(y-1)^2\right]\ln\left[x^2+(y-1)^2\right]+\left[(x-z)^2+y^2\right]\ln(x-z)^2+y^2]-\left[(x-z)^2+(y-1)^2\right]\ln\left[(x-z)^2+(y-1)^2\right], \quad (7)$$

$\tilde{x}_i=x_i/2a$ and $\tilde{y}_i=y_i/2a$, i=1,2.

The curves $\Delta W(\tilde{d})$ are given in Fig.7 for $\tilde{b}=10^{-3}$, $\alpha=\pi/200$, $\theta=\pi/300$, $\tilde{x}_1=-\tilde{x}_2=\tilde{y}_2=-1$, $\tilde{y}_1=2$ and different values of τ and q [125]. Depending on τ and q, the curves $\Delta W(\tilde{d})$ behave in quite different manners. When $q \le 5$ (e.g., see Fig.7a for q=1), they are similar to those considered in the previous section. When $q \ge 7$ (e.g., see Fig. 7b for q=10), some of them increase monotonously. One can conclude that for the given values of the parameters, the critical external shear stress τ_g is higher than for the case of GB disclination dipole splitting (Section 2.2.1).

Introducing (6) with (7) into the equation $\Delta W(\tilde{d}=\tilde{l})=0$, for $\tilde{d} << 1$ the authors [125] obtained

$$\frac{\tau_g}{D} \approx \tilde{b}q-\frac{\tilde{b}(\tilde{\alpha}+\tilde{\theta})}{4(1-\tilde{\alpha}-\tilde{\theta})}\left(1-2\ln\frac{\tilde{b}/\omega}{1-\tilde{\alpha}-\tilde{\theta}}\right)+(1-\tilde{\alpha}-\tilde{\theta})\frac{\omega^2}{4\tilde{b}}\left\{\tilde{\alpha}\Psi\left(\tilde{x}_1,\tilde{y}_1,\tilde{d}=\frac{\tilde{b}/\omega}{1-\tilde{\alpha}-\tilde{\theta}}\right)-\tilde{\theta}\Psi\left(\tilde{x}_2,\tilde{y}_2,\tilde{d}=\frac{\tilde{b}/\omega}{1-\tilde{\alpha}-\tilde{\theta}}\right)\right\}, \quad (8)$$

where $\tilde{\alpha}=\alpha/\omega$ and $\tilde{\theta}=\theta/\omega$. Three-dimensional plots $\tau_g(\tilde{\alpha},\tilde{\theta})$ are shown in Fig. 7c for q=10, $\tilde{x}_1=-\tilde{x}_2=\tilde{y}_2=-1$, $\tilde{y}_1=2$ and two values of the initial strength $\omega=\alpha+\beta+\theta$, ω = 0.01 and 0.05 [125]. It is seen that τ_g decreases when $\tilde{\alpha}$, $\tilde{\theta}$ and ω increase; that is again in accordance with intuition. When q=10, the numerical estimate for τ_g gave again the values of order G/1000-G/400.

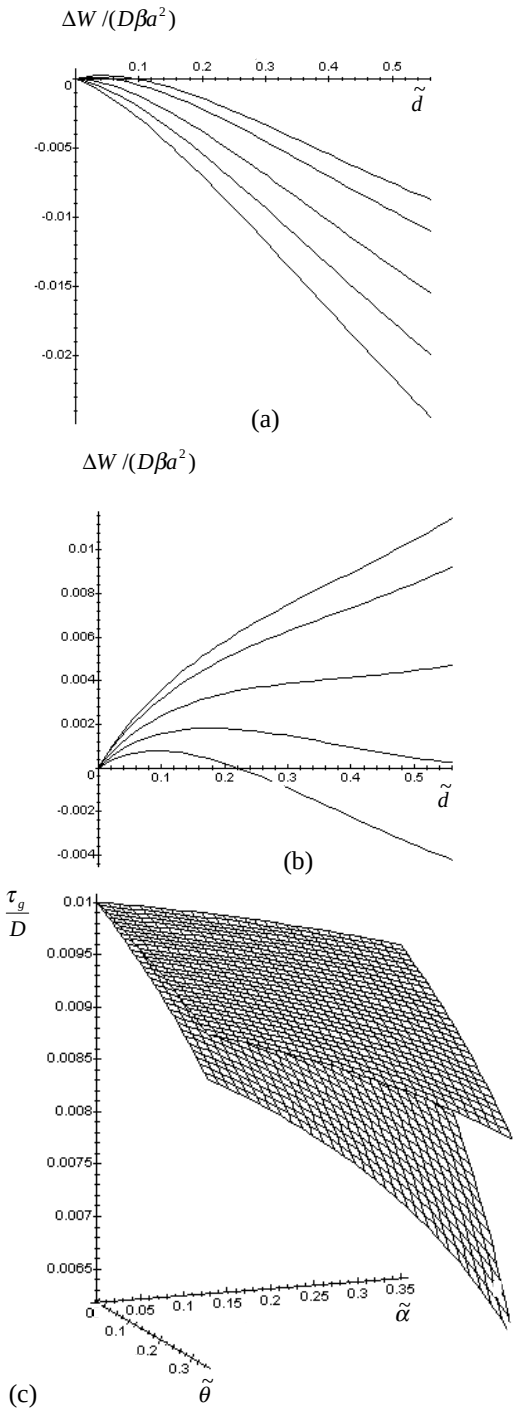

Fig. 7. Energy difference ΔW via the normalized misorientation band length $\tilde{d}$ (a, b) and critical shear stress τ_g/D via the normalized grain boundary disclination dipole strengths $\tilde{\alpha}$ and $\tilde{\theta}$ (c) for the model of a misorientation band being issued by a quadrupole-like disclination configuration localized at a grain boundary kink. The plots $\Delta W(\tilde{d})$ are given for the external shear stress τ/D=0, 0.001, 0.003, 0.005, and 0.007 (from top to bottom) for the two different values of the parameter q=1 (a) and 10 (b). The plots $\tau_g(\tilde{\alpha},\tilde{\theta})/D$ are shown for the initial disclination strength ω=0.01 (the upper surface) and 0.05 (the lower surface).

2.2.3. Splitting of an initial quadrupole-like disclination structure at a GB triple junction

Another more realistic model is a GB triple junction with a quadrupole-like disclination structure of the geometry shown in Fig.8 with d=0 [125]. Again this disclination configuration issues a mobile two-axes dipole of partial wedge disclinations having the strengths $\pm\beta$ and moving under the action of the GB disclination stress field as well as external shear stress τ. The new split configuration was suggested to consist of four two-axes disclination dipoles, one mobile (β-dipole) and three immobile (α-, θ- and γ-dipole). These three immobile dipoles are formed by the "central" negative triple-junction disclination having the strength $-\omega$ and three positive disclinations having the strengths $+\alpha$, $+\theta$ and $+\gamma$ and localized at the joined GBs. The relation $\omega = \alpha + \theta + \gamma$ must be valid.

The procedure of calculation of the difference in the total energies of the initial quadrupole-like disclination structure and new split configuration is absolutely similar to that described in Section 2.2.1. The final result is [125]

$$\Delta W = D\beta a^2\left\{4\tilde{d}\left(q\tilde{b}-\frac{\tau}{D}\right)-(2\alpha+\theta+\gamma)\left[(1+\tilde{d}^2)\ln(1+\tilde{d}^2)-\tilde{d}^2\ln\tilde{d}^2\right]-\theta\Psi(\tilde{x}_1,\tilde{y}_1,\tilde{d})-\gamma\Psi(\tilde{x}_2,\tilde{y}_2,\tilde{d})\right\}, \quad (9)$$

where the Ψ-function is given by (7). The dependences $\Delta W(\tilde{d})$ are plotten in Fig.9 for b=10^{-3}, $\alpha=\pi/300$, $\theta=\pi/100$, $\gamma=\pi/200$, $\tilde{x}_1=-\tilde{x}_2=\tilde{y}_2=\tilde{y}_1$=-1, and different values of τ and q [125]. This set of parameters gives the curves which are very similar to those considered in Section 2.2.1 (Fig.5) with the close values for the critical external stress τ_g when $q \geq 5$. In comparing these plots with those in Fig.7, one can conclude that both $\Delta W(\tilde{d})$ and τ_g depend on the concrete arrangement of the disclinations within the initial quadrupole-like disclination structure.

The substitution of (9) with (7) into the equation $\Delta W(\tilde{d}=\tilde{l})=0$ gives for $\tilde{d} << 1$ the following result [125]

$$\frac{\tau_g}{D}\approx\tilde{b}q-\frac{\tilde{b}(2\tilde{\alpha}+\tilde{\theta}+\tilde{\gamma})}{4(1-\tilde{\alpha}-\tilde{\theta}-\tilde{\gamma})}\left(1-2\ln\frac{\tilde{b}/\Omega}{1-\tilde{\alpha}-\tilde{\theta}-\tilde{\gamma}}\right)-(1-\tilde{\alpha}-\tilde{\theta}-\tilde{\gamma})\frac{\Omega^2}{4\tilde{b}}\left\{\tilde{\theta}\Psi\left(\tilde{x}_1,\tilde{y}_1,\tilde{d}=\frac{\tilde{b}/\Omega}{1-\tilde{\alpha}-\tilde{\theta}-\tilde{\gamma}}\right)+\tilde{\gamma}\Psi\left(\tilde{x}_2,\tilde{y}_2,\tilde{d}=\frac{\tilde{b}/\Omega}{1-\tilde{\alpha}-\tilde{\theta}-\tilde{\gamma}}\right)\right\}, \quad (10)$$

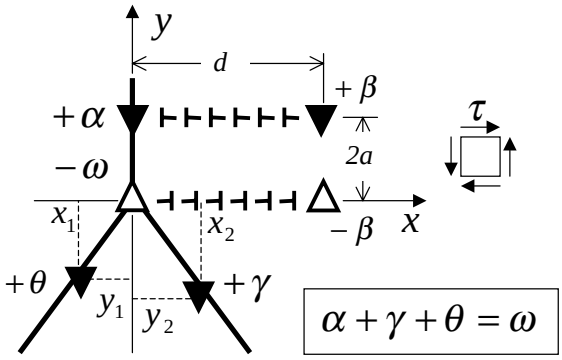

Fig. 8. Model of misorientation band generation by splitting of an initial quadrupole-like disclination configuration at a triple junction of grain boundaries.

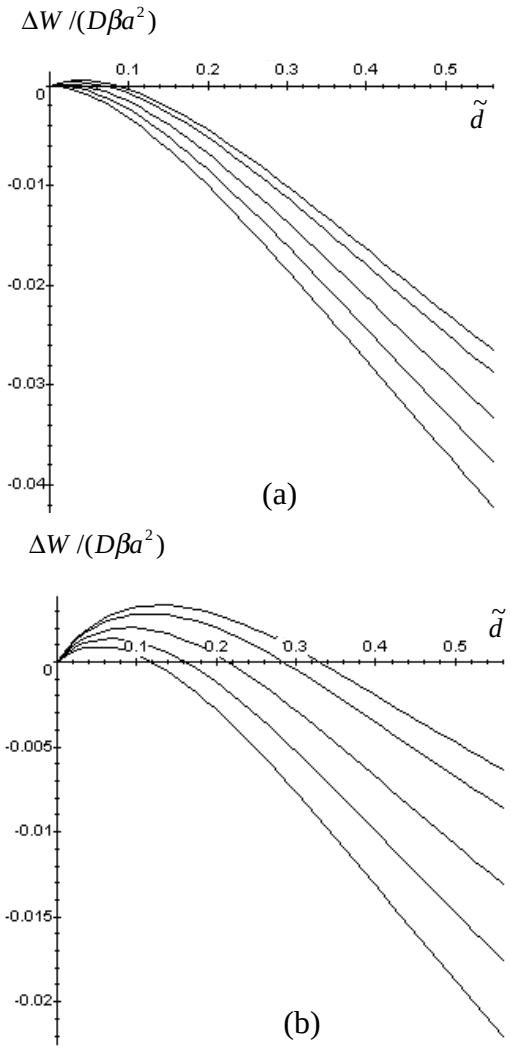

Fig. 9. Energy difference ΔW via the normalized length $\tilde{d}$ of a misorientation band being issued by a quadrupole-like disclination configuration localized at a triple junction of grain boundaries under the external shear τ/D=0, 0.001, 0.003, 0.005, and 0.007 (from top to bottom) for the two different values of the parameter q=1 (a) and 10 (b).

where $\tilde{\alpha}=\alpha/\Omega$, $\tilde{\theta}=\theta/\Omega$, $\tilde{\gamma}=\gamma/\Omega$, and $\Omega=\alpha+\beta+\theta+\gamma$ is the strength of the initial quadrupole-like disclination structure.

Using formula (10), the authors [125] investigated three-dimensional plots $\tau_g(\tilde{\alpha},\tilde{\theta})$ for different constant values of $\tilde{\gamma}$, $\tau_g(\tilde{\alpha},\tilde{\gamma})$ for those of $\tilde{\theta}$, and $\tau_g(\tilde{\theta},\tilde{\gamma})$ for those of $\tilde{\alpha}$ at the following parameter values: q=5, $x_1=-x_2=y_1=y_2=-1$, and two values of the initial disclination strength Ω. All the plots turned out to be very similar to those shown in Fig.7c and hence we do not represent them here. They demonstrated that τ_g decreases when $\tilde{\alpha}$, $\tilde{\theta}$, $\tilde{\gamma}$ and Ω increase [125]. When q=5 - 10, the numerical estimate for τ_g gave again values of the order G/1000-G/400.

2.3. Regimes of misorientation band propagation

In the previous sections, we have considered three different models of MB generation by using and analysing energy expressions (4), (6) and (9) for the limit of $\tilde{d}<<1$. To study further propagation of MBs, the authors [125] used the same expressions but for $\tilde{d}\geq 1$. Consider again the simplest model, i.e., the splitting of an initial GB disclination dipole (see Section 2.2.1, Fig.4).

The characteristic example of graphical representation of Eq. 4 for the case $\tilde{d}\geq 1$ is given in Fig.10 for $\alpha=\pi/200$, $b=10^{-3}$, $q=3$, and different values of the external shear stress τ [125]. Depending on the value of τ, the curves $\Delta W(\tilde{d})$ behave in different ways. When τ is smaller than some limiting quantity τ_p (e.g., $\tau_p\approx 0.003D$ for q=3), the curves $\Delta W(\tilde{d})$ are non-monotonous and achieve their minima, which determine equilibrium values of the MB length $\tilde{d}_{eq}$. When $\tau>\tau_p$, the curves $\Delta W(\tilde{d})$ goes with monotonous decrease and $\tilde{d}_{eq}$ is absent.

To find an analytical estimate for τ_p, one can solve the equation $\Delta W(\tau)=0$ for the limiting case $\tilde{d}\to\infty$ that gives [125]

$$\tau_p = Dq\tilde{b}. \qquad (11)$$

Obviously this provides the linear relation between τ_p and q, where q characterizes the effective surface energy of the misorientation boundaries.

The equilibrium length $\tilde{d}_{eq}$ is found from the standard equation $\frac{\partial \Delta W}{\partial \tilde{d}}=0$ with $\frac{\partial^2 \Delta W}{\partial \tilde{d}^2}>0$ and $\tilde{d}>1$. The final result reads [125]

$$\tilde{d}_{eq} \approx \frac{\alpha}{q\tilde{b}-\tau/D}, \qquad (12)$$

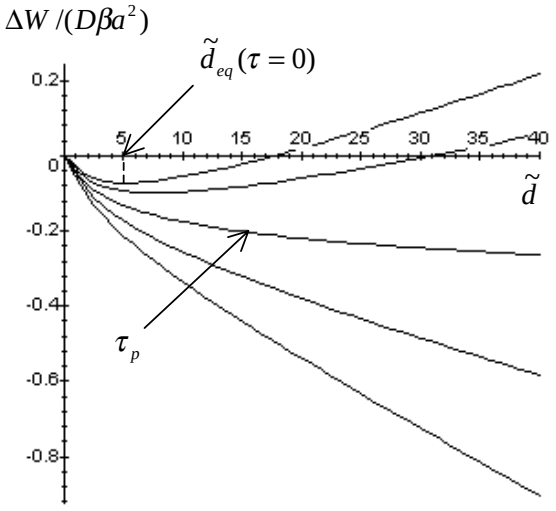

Fig. 10. Energy difference ΔW via the normalized length $\tilde{d}$ of a misorientation band being generated at a grain boundary disclination dipole and propagating far from it under the external shear stress τ/D=0, 0.001, 0.003, 0.005, and 0.007 (from top to bottom) for the parameter q=3.

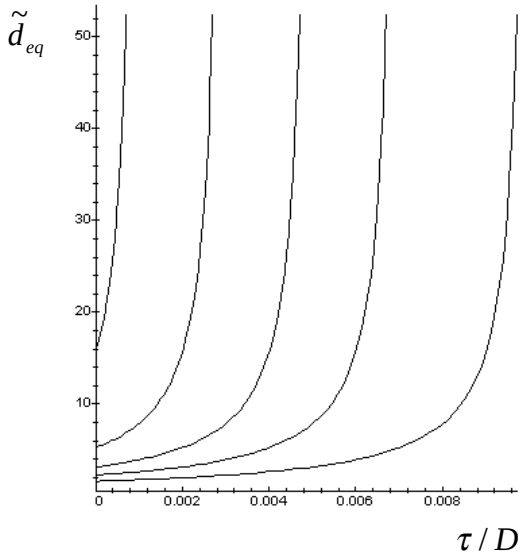

Fig. 11. Normalized equilibrium length, $\tilde{d}_{eq}$, of a misorientation band via the external shear stress τ/D for the different values of the parameter q=1, 3, 5, 7, and 10 (from top to bottom).

where $\tau<\tau_p$. The dependence of $\tilde{d}_{eq}$ on τ is illustrated in Fig. 11 for $\alpha=\pi/200$, $\tilde{b}$ = 10^{-3}, and different q. One can see that $\tilde{d}_{eq}$ increases with increasing τ and decreasing q.

It was thus shown in [125] that depending on the external shear stress τ, two main regimes of MB propagation are possible: stable and unstable propagation. When $\tau<\tau_p$, the MB propagation is stable and may be characterized by the equilibrium length $\tilde{d}_{eq}$. When $\tau>\tau_p$, the MB propagation is unstable and there is no equilibrium length. In reality, this means that the MB will propagate until it meets an obstacle like a GB or another MB (or some other defect configurations playing the role of obstacles) in which case the question of its further propagation must be considered again.

2.4. Computer simulation of dislocation- disclination interactions

To check and refine the models of MB propagation through an ensemble of edge dislocations as well as to calculate some important parameters of dislocation-disclination interactions (e.g., the effective length of dislocation capturing by a disclination dipole; this length was treated as the distance from a partial disclination line at which the corresponding edge dislocation must be stopped to provide the conservative motion "ahead" of the partial disclination), the method of 2D dislocation-disclination dynamics was used in [132]. This approach and some results were also quoted in [125].

The computer code objects were straight edge dislocations and straight wedge disclinations which could move within a two-dimensional rectangular box of an infinite elastically isotropic medium (Fig.12). Periodic boundary conditions were realized. The box sizes was chosen as 1x1 mm^2. The defect lines were normal to the box plane. The dislocations were characterized by their Burgers vectors b_x or b_y, coordinates $(x^{(i)},y^{(i)})$ and velocities$(\dot{x}^{(i)},\dot{y}^{(i)})$, where i=1 … n and n is the number of dislocations. All disclinations were arranged in dipole configurations which were assumed to be immobile and considered as sources of elastic fields. The dipoles were characterized by their strengths $\omega^{(j)}$, by the size and orientation of their arms and by the coordinates of the arm central points $(X^{(j)},Y^{(j)})$, where j = 1 … N and N is the number of disclination dipoles.

In such a computer model [132], the dislocations can move by gliding or climbing under the action of the total force due to external loading, elastic fields of other defects and dynamic friction. The dislocation dynamics is than ruled by Newton's law

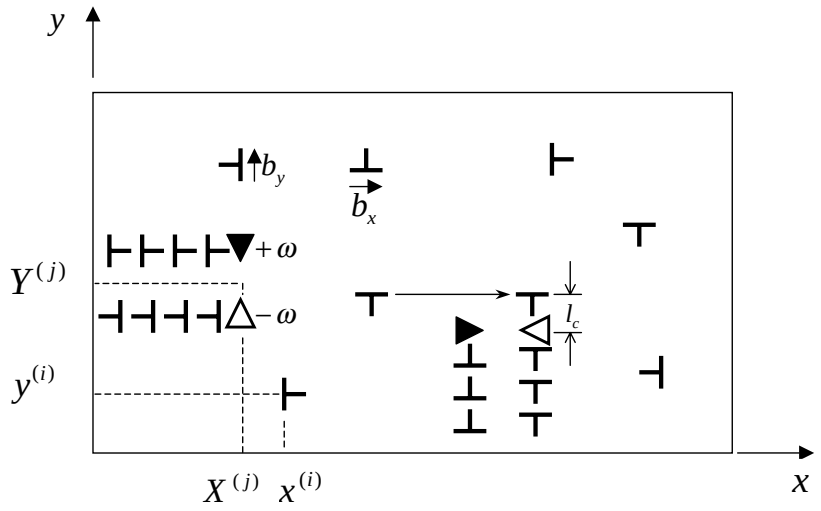

Fig. 12. 2D box for computer simulation of dislocation-disclination ensemble. The parameter l_c denotes the length of dislocation capturing by the disclination dipole.

$$m^{(i)}\ddot{x}^{(i)} = F_x^{(i)}, \tag{13}$$

$$m^{(i)}\ddot{y}^{(i)} = F_y^{(i)}, \tag{14}$$

where $m^{(i)}$ is the effective mass of the i-th dislocation, $\ddot{x}^{(i)}$ and $\ddot{y}^{(i)}$ are the x- and y-components of its acceleration, respectively. The p-component (p=x,y) of the resulting force on the i-th dislocation, $F_p^{(i)}$, is assumed to be a superposition

$$F_p^{(i)} = F_p^{def(i)} + F_p^{fr(i)} + F_p^{ext(i)} \tag{15}$$

with $F_p^{def(i)} = e_{mpl}\sigma_{lk}^{(i)}b_k^{(i)}s_m^{(i)}$ being the elastic force due to all other defects, $F_p^{fr(i)} = -\tau(v)b_p^{(i)}$ the dynamic friction force, and $F_p^{ext(i)} = \tau^{ext}b_p^{(i)}$ the external driving force. Here e_{mpl} denotes the permutation symbol, $\sigma_{lk}^{(i)}$ is the resulting elastic stress due to all other defects that is measured at the point where the ith dislocation is located, $b_k^{(i)}$ is the k-component of its Burgers vector, and $s_m^{(i)}$ is the m-component of the unit vector tangent to the dislocation line. All indexes p, m, l and k may denote x- or y-components. The shear stress $\tau(v)$ characterizes the crystalline lattice friction and depends on the dislocation velocity v. The external stress τ^{ext} is created by an external load applied to the solid.

Giving the initial coordinates and velocities of every defect, the system of motion equations (13)-(14) with (15) was solved numerically and the dependences of the coordinates x, y and the velocity components v_x and v_y on the time t were found.

The above approach was used to consider the elastic interaction of a gliding edge dislocation with a two-axes wedge disclination dipole in pure copper [132]. The module of the Burgers vector was taken as b_x = 0.256 nm, and hence the corresponding dislocation mass (per unit length of the dislocation) follows as $m=\rho b_x^2/2 \approx 1.4\cdot10^{-9}$ kg·m^{-1} (see [143], p.73). The position of a disclination dipole was fixed at the central point (X=500 μm, Y=500 μm) of the simulation box. In obtaining the following results, the force F_p^{ext} was neglected to catch the main features of elastic dislocation-disclination interactions as they are. The elastic force $F_p^{def}=\sigma_{xy}b_x$ was calculated with the disclination elastic stress field σ_{xy} taken from [8]. The dynamic friction force F_p^{fr} was taken as $F_p^{fr}(t)=-Bv(t)$, where B =1.7·10^{-5} Pa s that is characteristic for pure copper [144] (see also [143], p.76).

Some typical situations were studied for different orientations of the dipole arm, initial positions and velocities of the dislocation [125, 132]. It was shown that the dislocation behavior may strongly vary depending on the problem parameters. However, it is ruled mainly by the elastic stress field of the disclination dipole.

For example, consider a disclination dipole having the strength ω =0.01 and the arm $2a$ = 100 nm. Let the dislocation move with the initial velocity v_0=0.01 m s^{-1} quite far from the disclination dipole in the manner shown in Fig. 13 [125, 132]. The corresponding plots for the dislocation coordinate $x(t)$ (dashed line) and velocity $v(t)=\dot{x}(t)$ (solid line) are

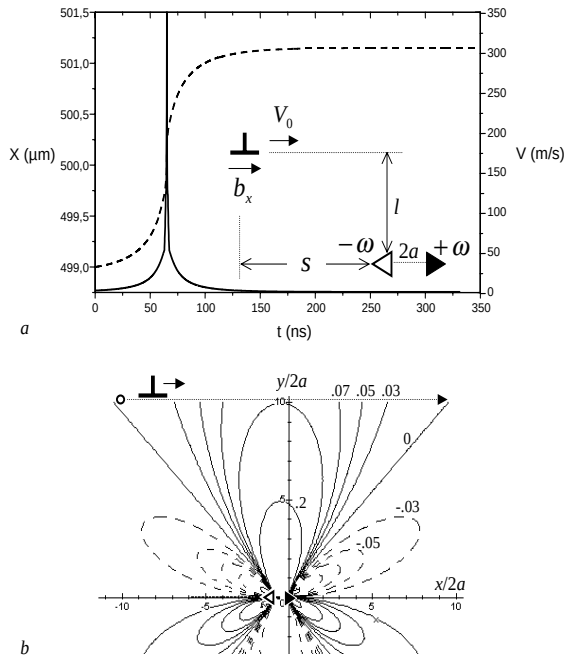

Fig. 13. Accelerated glide of an edge dislocation along the arm of a disclination dipole. The dashed and solid curves in plot (a) represent the dislocation position *x(t)* and velocity *v(t)*, respectively, when the dislocation glides in the field of the dipole positive long-range shear stress σ_{xy} (b). The calculations have been carried out for the following values of parameters: ω =0.01, b_x=0.256 nm, 2*a*=100 nm, *s*=1000 nm, *l* =1100 nm, x_0=499 μm, and v_0=0.01 m·s^{-1}.

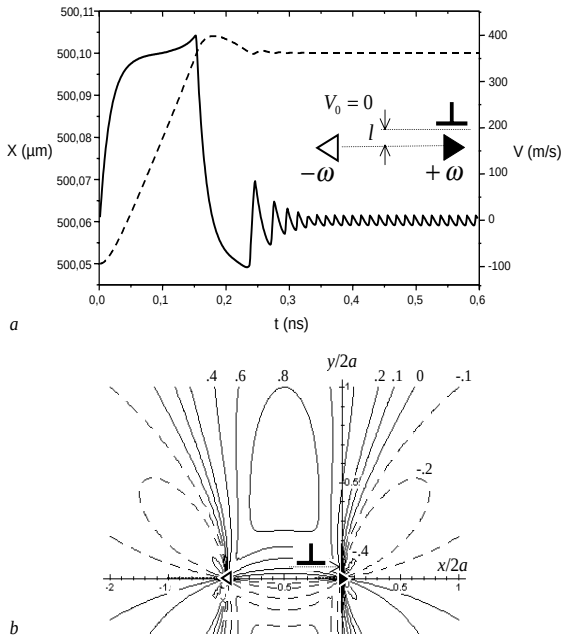

Fig. 14. Accelerated glide of an edge dislocation along the arm of a disclination dipole and capturing of the dislocation by the dipole. The dashed and solid curves in plot (a) represent the dislocation position *x(t)* and velocity *v(t)*, respectively, when the dislocation glides in the field of the dipole positive short-range shear stress σ_{xy} (b). The calculations have been carried out for the following values of parameters: ω=0.001, b_x=0.256 nm, 2*a*=100 nm, *s*=50 nm, *l* =1nm, x_0=500.05 μm, and v_0=0.

given in Fig.13a. In Fig.13b, the distribution of the dipole shear stress σ_{xy} in units of $D\omega$ is shown. The empty and black circles schematically denote in Fig.13b the initial and final dislocation positions, respectively. In fact, the dislocation starts to glide being under the action of positive shear stress σ_{xy} of the disclination dipole (the initial dislocation position is at the upper left corner in Fig.13b). As a result, the dislocation glides with an acceleration and its velocity becomes very high when it passes over the disclination dipole (Fig.13a), in the field of strongest disclination stresses (the upper central region in Fig.13b). At the same time, the friction force also achieves it maximum value. Therefore, when the dislocation has passed the region of maximum stress values over the dipole, its velocity starts to decrease fast. As a result, the dislocation moves away from the dipole with a negative acceleration until the point where the dipole stress turns to zero (the upper right region in Fig.13b). One can see there is no effect of dislocation capturing by the disclination dipole in this case.

The question arises: what are the problem conditions at which the dislocation capturing by the disclination dipole would be possible for a given defect configuration? The calculations [125, 132] demonstrated that the dislocation capturing is only possible when its initial position is just over the center of the disclination dipole, at a very small distance of it, and the disclination strength is very small. Thus, let the dislocation begin its motion just near the disclination dipole having the ten times lower strength ω =0.001 and the same arm (Fig.14). The dislocation is accelerated from v_0=0 within the region of the relatively higher positive shear stresses of the dipole (the initial dislocation position is at the central part of Fig.14b) and stopped after at the zero-value stress contour above the dipole, just near the positive disclination (see Fig.14b). This means that the disclination dipole has captured the dislocation.

However, the capturing occurs at very small distances from the dipole only. This distance (here l =1 nm) is much smaller than the spacing $l_c \approx b_x/\omega$ =256 nm between dislocations in the low-angle tilt walls whose edges are described by the disclination dipole (see Fig.12). Therefore, such a small capturing length can not provide the mechanism of conservative motion of a disclination dipole in direction normal to its arm by capturing or issuing edge dislocations.

The computer simulations [125, 132] show that the dynamics of the edge dislocation is totally ruled by the elastic field of the disclination dipole. The dislocation is accelerated when it appears in the region of increasing disclination stress, while further, when this field decreases, the dislocation is hampered by the force of dynamic friction and always stopped at the line of zero-level disclination shear stress. Thus, the dislocation behavior is determined by its initial position with respect to the disclination dipole and does not depend, in fact, on its initial velocity (at least for those velocity values which were used in simulations). The computer model [125, 132] approved that the two-axes dipole of wedge disclinations can move conservatively along the direction parallel to the dipole arm by means of capturing edge dislocations. However, the dipole motion along the normal to its arm cannot be explained correctly within the existing theoretical models and needs further investigation.

Based on the results of the theoretical models for MB generation and propagation considered in Section 2, one can make the following conclusions.

- Disclination models of MB generation at GB faults like kinks and GB junctions predict the existence of a critical external shear stress τ_g which is necessary for the MB generation events take place. The numerical estimate for the critical stress gives values of the order G/1000-G/400; the lower limit is in a good accordance with typical external stresses at the end of Stage II of deformation curves for conventional polycrystalline BCC and FCC metals, while the upper limit corresponds to the level of deforming stress observed in NCMs.
- The critical shear stress τ_g depends strongly on the geometry and strengths of initial GB disclination configurations, on the misorientation angle as well as on the effective surface energy of arising misorientation boundaries. It increases when the initial disclination strength decreases and the misorientation angle increases. The critical stress varies in direct proportion to the effective surface energy of misorientation boundaries.
- Disclination models of MB propagation predict the existence of a limiting external shear stress τ_p, which separates two main regimes of MB propagation: stable and unstable propagation. When the external stress is lower than the limiting stress, the MB propagation is stable and may be characterized by the equilibrium MB length which increases when the external stress increases and the effective surface energy of misorientation boundaries decreases. If the external stress is higher than the limiting stress, the MB propagation is unstable. The limiting external stress varies in direct proportion to the effective surface energy of misorientation boundaries.
- Computer simulations by means of a 2D dislocation-disclination dynamics code have shown that the existing models of the disclination dipole motion must be reconsidered with taking into account the conclusion that the disclination dipole cannot move concervatively along the normal to its arm by capturing edge dislocations.

3. MOTION OF GRAIN BOUNDARY DISCLINATIONS

Transformations of GBs often strongly influence both the structure and the properties of polycrystalline and nanocrystalline materials, e.g. [8, 20, 26, 74, 75, 78, 107, 114, 145-173]. In particular, changes of misorientation parameters of GBs, that are capable of resulting in grain rotations, have been experimentally detected in polycrystalline and nanocrystalline materials under (super)plastic deformation (see, e.g. [152-156]). Ke *et al.* [168, 169] observed *in situ* that plastic deformation of nanocrystalline gold films with the grain size d<25 nm occured through GB sliding and grain rotation near the tips of opening cracks. Noskova et al. [170-172] have also reported about *in situ* TEM observation of GB sliding and grain rotation in nanocrystalline pure metals (Cu, Ni and Ti with grain size d=20-40 nm) and $Fe_{73.5}Cu_1Nb_3Si_{13.5}B_9$ alloy (with grain size $d \approx 10$ nm) under active unidirectional tension with strain rate 10^{-5} s^{-1}. It is important that rotation of grains does not always need to apply an external mechanical load. Sometimes it is enough to carry out a special thermal treatment. For example, grain rotations have been observed experimentally in thin films of gold under thermal treatment [173].

According to contemporary theoretical representations of GBs, changes of their misorientation parameters occur via motion of GB disclinations [8, 26, 174]. Such disclinations are intensively gener-

ated in polycrystals and NCMs under highly nonequilibrium conditions of their fabrication. These conditions are typical for the technologies of intensive plastic deformation and ball milling that give submicro- and nanostructured materials with nonequilibrium GBs containing GB and triple junction disclinations [23, 25, 27, 126, 140] (see also Section 2). It is quite natural that in such NCMs, like in conventional polycrystals under large deformation, the processes of rotational deformation are assumed to be realized by means of concervative motion of disclination dipoles [125, 175-177].

Motion of GB disclinations in plastically deformed materials is commonly treated as that associated with absorption of lattice dislocations (that are generated and move in grains under the action of mechanical load) by GBs [8, 156]. This micromechanism, according to paper [156], is responsible for experimentally observed grain rotations in fine-grained materials during (super)plastic deformation. However, the consequent motion of a GB disclination along a GB requires processes of the dislocation absorption to be well ordered in space and time. In particular, lattice dislocations with certain Burgers vectors have to reach the GB in only vicinity of the disclination that moves along the boundary due to acts of absorption of these dislocations. This is in an evident contradiction with the fact that sources of lattice dislocations in plastically deformed materials are commonly distributed in a rather irregular way within a grain and, therefore, are not capable of providing the regular flow of dislocations to the disclination moving along a GB. Moreover, in the situation with grain rotations in thin films of gold under thermal treatment [173], absorption of lattice dislocations by GBs hardly plays an important role in changes of GB misorientation parameters, because the dislocation density in grain interiors is too low to cause grain rotations.

Based on these conclusions, the alternative theoretical models [176-179] have been proposed. These models have used the idea that GB disclinations can move along GBs due to emission (in contrast to absorption [156]) of lattice dislocations from GBs into adjacent grain interiors. It has also been assumed that the GB disclinations are partial, i.e. they may be represented as ragged walls of edge dislocations [8, 133] (this assumption is always valid in practice), and accordingly wedge in nature. In this case, a GB disclination can emit a pair of edge lattice dislocations with the Burgers vectors corresponding to the glide systems in the adjacent grains. The sum of these lattice Burgers vectors are supposed to be equal to the Burgers vector of a GB dislocation from the ragged wall (strictly speaking, this condition is not necessary and has been taken for the sake of simplicity; one could also include into consideration a difference GB dislocation whose Burgers vector would compensate a possible disparity). The emission of dislocation pairs permits the GB disclination to move conservatively along the GB, and the events of dislocation emission are determined by the conditions at the GB disclination. We consider below the main results of the models [176-179] which describe the rotational mode of plastic deformation in fine-grained materials as that which is realized through conservative motion of dipoles of GB disclinations emitting pairs of lattice dislocations.

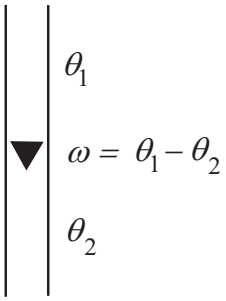

Fig. 15. Grain boundary disclination (black triangle) separates boundary fragments characterized by different values, θ_1 and θ_2, of tilt misorientation.

3.1. Changes in grain boundary misorientation

Following the theory of GBs, two fragments of a GB that are characterized by different values of tilt misorientation parameter are divided by the line of a GB disclination [8, 26, 114, 174]. More precisely, the line that separates the two boundary fragments with tilt misorientation parameters θ_1 and θ_2, respectively, is described as the line of a GB wedge disclination with strength $\omega=\theta_1-\theta_2$ (Fig.15). In the framework of the discussed representations, evolution (in time) of tilt misorientation along GBs is treated as that related to the motion of GB disclinations.

In the framework of the model [178, 179], an elementary act of transfer (by distance l) of a GB disclination with strength ω is accompanied by emission of two lattice dislocations with Burgers vectors $\vec{b}_1$ and $\vec{b}_2$ from the GB into the adjacent grains I and II, respectively (Fig.16). The disclination

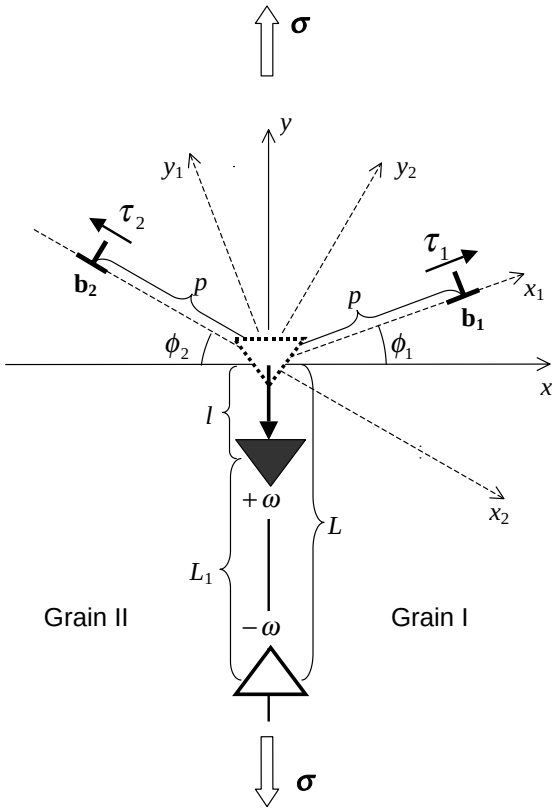

Fig. 16. Displacement of the wedge disclination (black triangle) with the strength ω from its initial position (dashed triangle) by the distance *l* is accompanied by the emission of two lattice dislocations with Burgers vectors $\vec{b}_1$ and $\vec{b}_2$. The ω-disclination moves along the grain boundary plane (which is perpendicular to the figure plane and intersects it along the *y*-axis) towards another disclination (white triangle) with the strength -ω. The *x*-axis is normal to the grain boundary plane. The x_1y_1 and x_2y_2 coordinate systems are associated with the gliding planes of emitted dislocations. ϕ_1 and ϕ_2 are the angles between the normal to the grain boundary plane and the gliding planes of respectively the first and the second dislocations. τ_1 and τ_2 are the shear stresses acting along the gliding planes of the first and second dislocation, respectively. *L* and L_1 are the distances between the disclinations before and after displacement of the ω-disclination.

with strength ω can be treated as that terminating a ragged wall of periodically spaced GB dislocations with identical Burgers vectors $\vec{b}$ and spacing (period) *l*. This dislocation representation is relevant to both small- and large-angle GBs with GB dislocations having a "large" crystal lattice Burgers vector in the case of small-angle GBs and a "small" DSC-lattice Burgers vector in the case of large-angle GBs [146, 180]. With the spacing *l* between such dislocations assumed to be the distance of an elementary transfer of the disclination, Burgers vectors of the GB dislocations and strength ω of the GB disclination obey the equations: $\vec{b}_1 + \vec{b}_2 = \vec{b}$ and $|\vec{b}| = b \approx l\omega$. From the former equation, one finds that the Burgers vector magnitude *b* is in the following relationship with the magnitudes, b_1 and b_2, of Burgers vectors of the emitted dislocations:

$$b = b_1\left(\cos\phi_1 + \frac{b_2}{b_1}\cos\phi_2\right) = b_1\frac{\sin(\phi_1+\phi_2)}{\sin\phi_2}, \qquad (16)$$

where ϕ_1 and ϕ_2 are the angles between the normal to the GB plane and the gliding planes of the respectively first and second emitted lattice dislocations (Fig.16). Notice that $b < b_1, b_2$ in the case of large-angle GBs (containing dislocations with DSC-lattice Burgers vectors).

The consequent emission of lattice dislocation pairs (Fig.16) causes change of GB misorientation along large fragments of the GB plane. This process is capable of giving rise to the rotation of a grain as a whole.

The above model is approximate. First, the authors [178, 179] have restricted their consideration to the *z*-independent situation with a disclination dipole at a tilt boundary characterized by two macroscopic geometric parameters, the angles ϕ_1 and ϕ_2 (Fig.16). However, tilt boundaries which are effectively described in terms of disclinations [8], represent the most widespread type of GBs in real materials, in which case this model covers most real GBs. Second, the choice of the disclination dipole as a subject of the theoretical analysis (addressed the GB disclination motion) in this model has been related to the two following aspects: (i) the long-range stress field of the moving disclination should be screened, and (ii) there is an experimental evidence (see reviews [8, 114] and references therein) that disclinations form dipole, quadrupole and multipole configurations in real materials under large deformation. In principle, one could consider an individual GB disclination whose elastic fields would be screened by outer boundaries of the solid as was the case in works [20, 181-183]. Such a consideration is sometimes reasonable but always significantly more complicated. That is why the authors [178, 179] have chosen the simplest way to

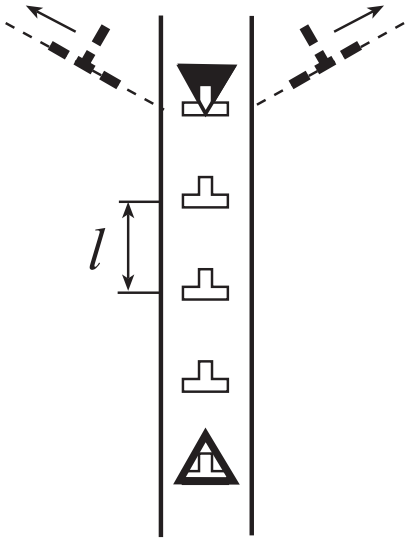

Fig. 17. Disclinations composing a dipole terminate a ragged wall of periodically (with period *l*) spaced grain boundary dislocations with either a crystal-lattice or DSC-lattice Burgers vector in respectively small- and large-angle boundaries. An elementary transfer of a moving disclination, shown in Fig. 16, is accompanied by the splitting of one of the grain boundary dislocations into the two lattice dislocations.

screen the long-range stress field of the moving (first) disclination by using the simplest self-screened disclination configuration (disclination dipole) among others which are observed in real materials. Third, it has been supposed that the disclination dipole consists of mobile (first) and immobile (second) disclinations (Fig.16). As with the first disclination, the second disclination may also represent the discontinuity of misorientation across the GB, or may be a triple junction disclination, etc. It may also be as mobile as the first disclination is. This would not change results of the model, because the authors [178, 179] have analysed only the energetic possibility for an elemental displacement of the first disclination. It would hardly be expected that both the disclinations must make such elemental "jumps" simultaneously. Therefore, one can treat one of them as "mobile" while another one as "immobile".

Following papers [178, 179], let us consider energetic characteristics of the GB disclination motion under discussion (Fig.16). The dipole of the GB disclinations can be treated as the defects terminating the GB dislocation wall of finite extent (Fig.17), in which case an elementary transfer of the moving disclination occurs via the splitting of one GB dislocation belonging to the wall into two lattice dislocations. The motion of the GB disclination occurs under the action of external mechanical load which, in the framework of the model, causes uniaxial stress parallel with the GB plane and promotes the motion of the emitted dislocations (Fig.16). The elementary transfer of a GB disclination by distance *l*, accompanied by emission of two lattice dislocations, is energetically favourable, if the energy (per unit disclination length) W_2 of the defect configuration resulted from the transfer is lower than the energy W_1 of the pre-existent configuration (before the transfer): $\Delta W = W_2 - W_1 < 0$.

The pre-existent configuration represents a dipole of GB disclinations with the distance *L* (the dipole arm) between them. The energy W_1 of this system is given by

$$W_1 = E_d = \frac{D\omega^2 L^2}{2}\left(\ln\frac{R}{L} + \frac{1}{2}\right) + NE_b^c, \qquad (17)$$

where the first term is the strain energy of the disclination dipole (see formula (1) in Section 2.2.1) and the second term is the sum energy of cores of the *N* GB dislocations which compose the ragged wall (Fig.17). The core energy is approximated as [141] $E_b^c \approx Db^2/2$.

The energy density W_2 of the dipole configuration resulted from the elementary transfer (Fig.16) can be written as follows [178, 179]:

$$W_2 = E_d^{'} + E_{b_1} + E_{b_2} + E_d^{b_1} + E_d^{b_2} + E_{b_2}^{b_1} + E_\sigma^{b_1} + E_\sigma^{b_2}. \qquad (18)$$

Here $E_d^{'}$ denotes the strain energy of the resultant disclination dipole characterized by the dipole arm $L_1 = L - l$, E_{b_1} (E_{b_2}) the self energy of the first (second) emitted dislocation, $E_d^{b_1}$ ($E_d^{b_2}$) the energy that characterizes elastic interaction between the first (second) emitted dislocation and the disclination dipole, $E_{b_2}^{b_1}$ the energy that characterizes elastic interaction between the emitted dislocations, and $E_\sigma^{b_1}$ ($E_\sigma^{b_2}$) the work of the external stress σ spent to transfer the first (second) dislocation to its position shown in Fig.16.

The strain energy $E_d^{'}$ of the disclination dipole with the arm L_1 is given by formula (17) with the substitution of *L* for L_1 and *N* for (*N*-1).

The self energies of the dislocations read [141]

$$E_{b_i} = \frac{Db_i^2}{2}\left(\ln\frac{R}{r_c} + 1\right), \qquad (19)$$

where i=1,2, and r_c is the dislocation core radius (which is assumed to be the same for both the dislocations under consideration).

Calculation of the other terms of the sum (18) is given in paper [179]. The final expressions for the energies $E_d^{b_i}$, $E_{b_2}^{b_1}$, and $E_\sigma^{b_i}$ are as follows:

$$E_d^{b_i} = \frac{D}{2}\omega b_i \cos\phi_i \left(L \ln \frac{R^2 + L^2 + 2RL\sin\phi_i}{p^2 + L^2 + 2pL\sin\phi_i} - l \ln \frac{R^2 + l^2 + 2Rl\sin\phi_i}{p^2 + l^2 + 2pl\sin\phi_i} \right), \quad (20)$$

$$E_{b_2}^{b_1} = \frac{D}{2} b_1 b_2 \left(1 + \cos(\phi_1 + \phi_2) \ln \frac{p^2 + R^2 + 2pR\cos(\phi_1 + \phi_2)}{2ep^2\left[1 + \cos(\phi_1 + \phi_2)\right]} - \frac{2pR\sin^2(\phi_1 + \phi_2)}{p^2 + R^2 + 2pR\cos(\phi_1 + \phi_2)} \right), \quad (21)$$

$$E_\sigma^{b_i} = -\frac{\sigma}{2} b_i p \sin 2\phi_i, \quad (22)$$

where e is the base of the natural logarithm and σ is the external normal stress (Fig.16). With formulae (17)-(22), the authors [178, 179] have found the difference ΔW:

$$\Delta W = \frac{D}{2}\left\{ \left(b_1^2 + b_2^2\right)\left(\ln\frac{R}{r} + 1 \right) - b^2 - \frac{\sigma}{D} p\left(b_1 \sin 2\phi_1 + b_2 \sin 2\phi_2\right) + b_1 b_2 \left(1 + \cos(\phi_1 + \phi_2) \ln \frac{p^2 + R^2 + 2pR\cos(\phi_1 + \phi_2)}{2ep^2\left[1 + \cos(\phi_1 + \phi_2)\right]} - \frac{2pR\sin^2(\phi_1 + \phi_2)}{p^2 + R^2 + 2pR\cos(\phi_1 + \phi_2)} \right) + \omega^2 L_1^2 \left[\ln\frac{R}{L_1} + \frac{1}{2} - \frac{L^2}{L_1^2}\left(\ln\frac{R}{L} + \frac{1}{2} \right) \right] + \omega \sum_{i=1}^{2} b_i \cos\phi_i \left(L \ln \frac{R^2 + L^2 + 2RL\sin\phi_i}{p^2 + L^2 + 2pL\sin\phi_i} - l \ln \frac{R^2 + l^2 + 2Rl\sin\phi_i}{p^2 + l^2 + 2pl\sin\phi_i} \right) \right\}. \quad (23)$$

Formula (23) has allowed to numerically investigate the dependences of ΔW on parameters, p, ϕ_1, ϕ_2, σ, R, and L, of the system under consideration. Thus, the dependences $\Delta W(p)$ are shown in Fig.18 for various values of characteristic angles ϕ_1 and ϕ_2 related to the crystallography of the adjacent grains [179]. These dependences indicate that angles ϕ_1 and ϕ_2 crucially influence elementary transfer of a GB disclination. In fact, the disclination transfer is energetically facilitated at low angles and hampered with rising ϕ_1 and ϕ_2. At large values of ϕ_1 and ϕ_2 (tentatively >50 °) there exists an energetic barrier for motion of the emitted lattice dislocations, and the disclination transfer is energetically unfavourable. In the range of ϕ_1 and ϕ_2 from 0° to tentatively 20 °, the dislocation motion has a barrier-less character with ΔW (<0) decreasing with rising the dislocation path p (Fig.18). In the range of ϕ_1 and ϕ_2 from tentatively 20° to 50°, the disclination transfer is either favourable or unfavourable, depending on other parameters (L, ω, σ) of the system. In this situation, the characteristic energy difference $\Delta W(p=b)$ at the starting point of the dislocation motion is highly sensitive to both the distance L between the disclinations and their strength magnitude ω (see Figs.19 and 20) [178, 179].

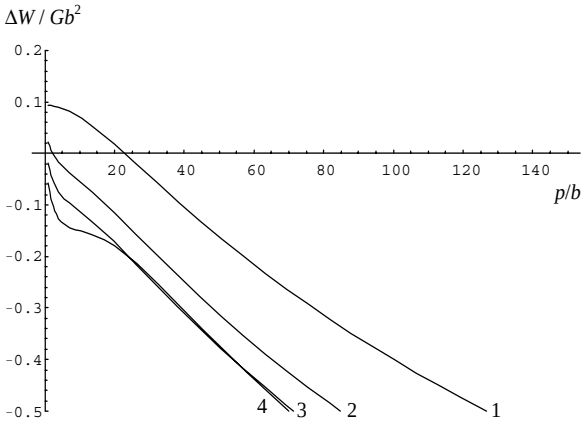

Fig. 18. Dependence of ΔW on the distance p moved by each of the emitted lattice dislocations, for L=30b, σ =10^{-3}G, R=10^5b, ω=0.1, and the following values of the characteristic angles: ϕ_1=ϕ_2=45° (curve 1), ϕ_1=30° and ϕ_2=40° (curve 2), ϕ_1=20° and ϕ_2=30° (curve 3), and ϕ_1=ϕ_2=2° (curve 4).

At the same time, $\Delta W(p=b)$ weakly depends on the external stress σ (see Fig.21) [179]. The influence of the stress σ on the characteristic energy difference $\Delta W(p)$ increases with rising the dislocation path p at some intermediate values (close to 45°) of angles ϕ_1 and ϕ_2. The energy difference $\Delta W(p)$ at low values of angles ϕ_1 and ϕ_2 is weakly

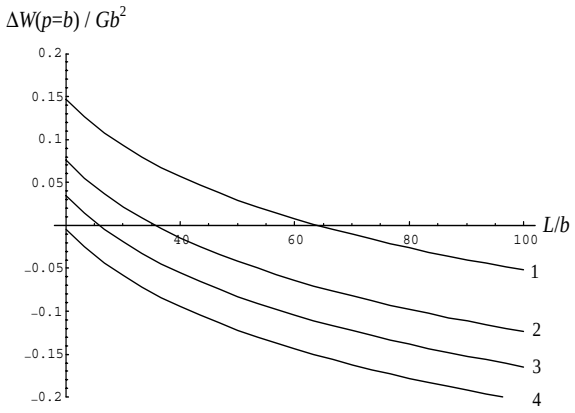

Fig. 19. Dependence of ΔW on the distance L between grain boundary disclinations at the initial stage of the dislocation emission (at $p=b$), for $\sigma = 10^{-3}G$, $R=10^5 b$, $\omega=0.1$, and the following values of the characteristic angles: $\phi_1=\phi_2=45°$ (curve 1), $\phi_1=30°$ and $\phi_2=40°$ (curve 2), $\phi_1=20°$ and $\phi_2=30°$ (curve 3), and $\phi_1=\phi_2=2°$ (curve 4).

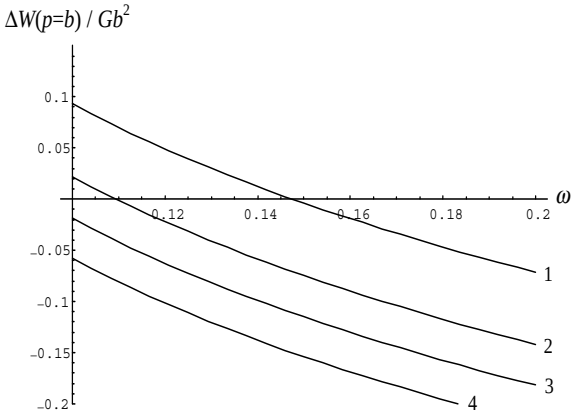

Fig. 20. Dependence of ΔW on the disclination strength ω at the initial stage of the dislocation emission (at $p=b$), for $\sigma=10^{-3}G$, $R=10^5 b$, $L=30b$, and the following values of the characteristic angles: $\phi_1=\phi_2=45°$ (curve 1), $\phi_1=30°$ and $\phi_2=40°$ (curve 2), $\phi_1=20°$ and $\phi_2=30°$ (curve 3), and $\phi_1=\phi_2=2°$ (curve 4).

sensitive to σ, as is shown in Fig. 22 [179]. This naturally follows from the geometry of the system (Fig.16).

Thus, probability of splitting of a GB dislocation into a pair of lattice dislocations, their emission and corresponding motion of the GB disclination increases with decreasing values of angles ϕ_1 and ϕ_2, and with growth of the dipole arm L and disclination strength ω. The GB disclination motion has been proved to be an energetically favourable process in rather wide ranges of parameters that characterize the defect configuration under consideration. In contrast to the previously considered situation with disclination motion associated with (ordered in space and time) absorption of dislocations by GBs [8, 156], the model of disclination motion associated with emission of dislocation pairs [178, 179] does not require any correlated flux of dislocations from grain interiors to GBs. The suggested micromechanism for the disclination motion (Fig.16) can be responsible for experimentally observed rotations of grains in fine-grained materials under (super)plastic deformation and thermal treatment.

3.2. Motion of dipole of grain boundary disclinations

The model of motion of a GB disclination [178, 179] (discussed in the previous Section) is easily to extend to the case of conservative motion of a dipole of such disclinations under the action of external

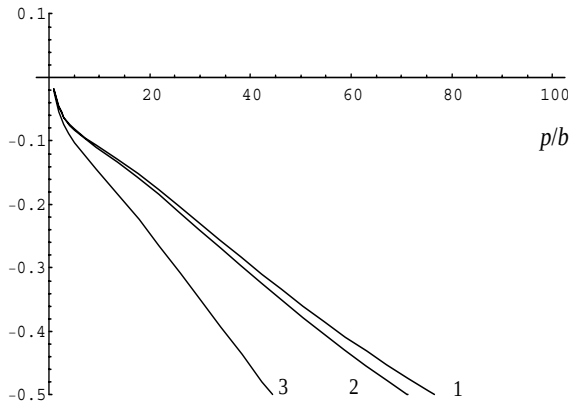

Fig. 21. Dependence of ΔW on the distance p moved by the emitted dislocations, for $\phi_1=30°$ and $\phi_2=40°$, $R=10^5 b$, $L=30b$, $\omega=0.1$, and the following values of the applied stress $\sigma/G=10^{-4}$, 10^{-3} and 10^{-2} (curves 1, 2 and 3, respectively).

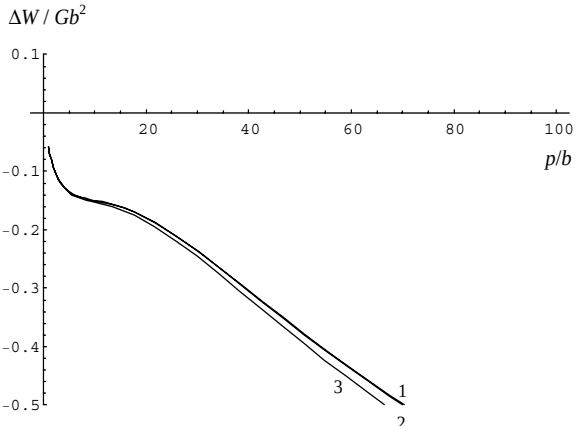

Fig. 22. Dependence of ΔW on the distance p moved by the emitted dislocations, for $\phi_1=\phi_2=2°$, $R=10^5 b$, $L=30b$, $\omega=0.1$, and the following values of the applied stress $\sigma/G=10^{-4}$, 10^{-3} and 10^{-2} (curves 1, 2 and 3, respectively).

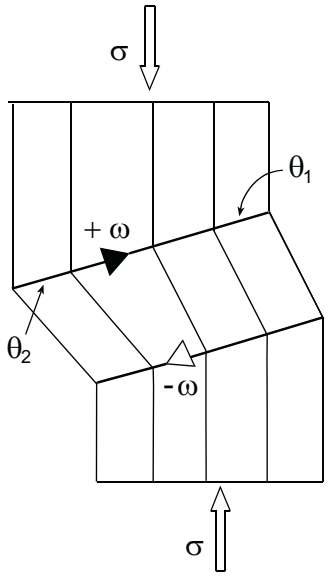

Fig. 23. Motion of a disclination dipole may be considered as similar to the motion of a (super)dislocation.

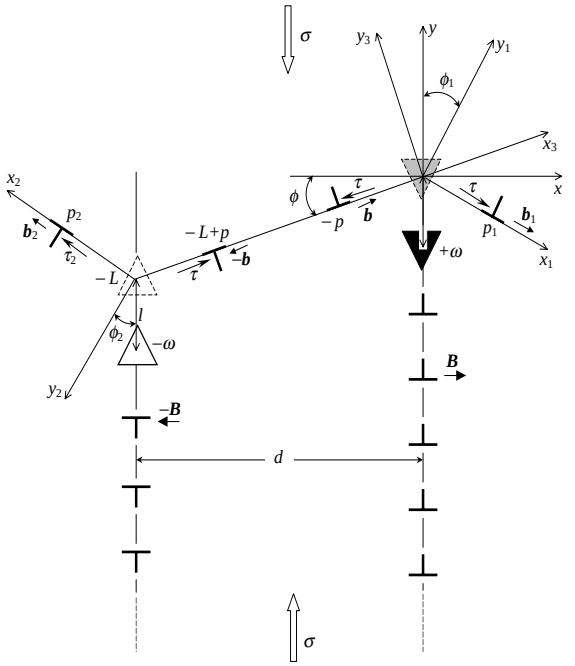

Fig. 24. Motion of a dipole of grain boundary disclinations is accompanied by emission of lattice dislocations from the grain boundaries into the adjacent grains. The dislocation slip planes are inclined at the angles ϕ, ϕ_1 and ϕ_2 to the *x*-axis.

loading [176, 177]. Motion of dipoles of the GB disclinations may be considered as similar to the motion of (super)dislocations and essentially contributes to high-strain deformation (Fig.23) [8]. Remember that experimental evidence of the existence of disclination dipoles in typical NCMs has recently been demonstrated in direct atomic-level HREM observations by Murayama et al. [126].

Following the model [176, 177], one can assume that the rotational deformation in a fine-grained material occurs via the stress-induced motion of a dipole of GB disclinations. In the framework of the model, the dipole consists of two GB disclinations with the strengths +ω and -ω, respectively, and has the arm *L*. The disclination of the strength +ω (+ω-disclination) transfers by the distance *l* due to the emission of two lattice dislocations with the Burgers vectors $\vec{b}$ and $\vec{b}_1$ into the adjacent grains (Fig.24) [176, 177]. The dislocation with the Burgers vector $\vec{b}$ moves along its gliding plane towards the disclination of the strength -ω (-ω-disclination). This disclination moves by the distance *l* in the same direction as the +ω-disclination due to the emission of two lattice dislocations with the Burgers vectors $-\vec{b}$ and $\vec{b}_2$ into the abutting grains. The dislocations with the Burgers vector $\vec{b}$ and $-\vec{b}$ emitted by the +ω- and -ω-disclinations, respectively, meet each other and annihilate.

Of course, this model is very idealistic, even more than that considered in Section 3.1. In a real NCM fabricated by severe deformation method, the GB disclinations with various values of strength are distributed in a rather disordered manner along non-equilibrium GBs and the emitted lattice dislocations do not necessary annihilate. In addition, grain interiors of a fine-grained material contain many lattice dislocations generated during severe plastic deformation. These dislocations are capable of interacting and annihilating with the dislocations emitted by GB disclinations. Thus, real processes occurring during motion of GB disclinations can be very complicated and different from those described by the model [176, 177]. However, this simplified model is convenient for a strict mathematical analysis and effective for understanding the key peculiarities of the GB disclination motion accompanied by emission of lattice dislocations. Also, it can serve as a basis for further detailed consideration of evolution of GB defects in plastically deformed NCMs.

The cooperative motion of the GB disclinations composing the dipole causes the plastic deformation of a NCM. The dipole motion is energetically favourable, if the difference between the system energies (per unit disclination length) after (W_2) and before (W_1) the dipole elementary transfer is negative: $\Delta W=W_2-W_1<0$. The corresponding calculation

of ΔW is very similar to that described in Section 3.1, so we give below only several intermediate formulae and the final result. The full calculation procedure is represented in paper [176].

The energy of the system in its initial state (before the dipole transfer) W_1 is the strain energy of the disclination dipole which is given by the first term in formula (17).

The disclination dipole motion is accompanied by the emission of the lattice dislocations, in which case the energy density W_2 of the defect system consists of the five following terms [176, 177]:

$$W_2 = E_d + E_{b_1} + E_{b_2} + E_{bb} + E_{\text{int}}. \qquad (24)$$

Here $E_d=W_1$ is the strain energy of the disclination dipole which does not change during its correlated motion, E_{b1} and E_{b2} are the self energies of the emitted dislocations with the Burgers vectors $\vec{b}_1$ and $\vec{b}_2$, respectively; E_{bb} is the self energy of the dislocation dipole consisting of the emitted dislocations with Burgers vectors $\vec{b}$ and -$\vec{b}$, and E_{int} is the sum energy that characterizes all the interactions between the defects composing the system (Fig.24) (except between both the disclinations whose interaction energy is included in E_d, and between the $\vec{b}$- and $\vec{b}$-dislocations whose interaction energy is included in E_{bb}), and between the defects and the applied stress σ. The last component can be decomposed into nine terms as follows [176]:

$$E_{\text{int}} = E_d^{b_1} + E_d^{b_2} + E_d^{bb} + E_{b_2}^{b_1} + E_{bb}^{b_1} + E_{bb}^{b_2} + E_\sigma^{b_1} + E_\sigma^{b_2} + E_\sigma^{bb}. \qquad (25)$$

Here $E_d^{b_1}$, $E_d^{b_2}$ and E_d^{bb} denote the energies that characterize the interaction of the disclination dipole with respectively the $\vec{b}_1$- and $\vec{b}_2$-dislocations, and the dipole of $\pm\vec{b}$-dislocations; $E_{b_2}^{b_1}$ is the energy of the interaction between the $\vec{b}_1$- and $\vec{b}_2$-dislocations; E_{bb}^{b1} and E_{bb}^{b2} denote the energies that characterize the interaction of the dislocation dipole with these dislocations; $E_\sigma^{b_1}$, $E_\sigma^{b_2}$ and E_σ^{bb} are the energies that characterize the interaction of the applied stress σ with respectively the emitted $\vec{b}_1$- and $\vec{b}_2$-dislocations, and the dislocation dipole. Consider the energies figuring on the r.h.s. of formula (24) with account for (25).

The self energies of the $\vec{b}_1$- and $\vec{b}_2$-dislocations are given by formula (19).

The self energy of the dipole of $\pm\vec{b}$-dislocations is calculated as the work spent to generate these dislocations in their sum elastic field that finally gives [176]

$$E_{bb} = Db^2\left(\ln\frac{|L-2p-r_c|}{r_c}+1\right), \qquad (26)$$

where the last term "1" is added to take into account the contributions of the dislocation cores.

The energies of interaction between the disclination dipole and the lattice dislocations are calculated in a similar way, as the work spent to generate these dislocations in the stress field of the disclination dipole. In doing so, one has to use the different coordinate systems shown in Fig.24. These quite cumbersome calculations result in [176]

$$E_d^{b_1} = \frac{D\omega b_1}{2}\Psi(p_1,\phi,\phi_1), \qquad (27)$$

$$E_d^{b_2} = \frac{D\omega b_2}{2}\Psi(p_2,-\phi,-\phi_2), \qquad (28)$$

$$E_d^{bb} = -\frac{D\omega bl}{2}\times \cos\phi\ln\frac{(L-p)^4+l^4+2(L-p)^2l^2\cos 2\phi}{p^4+l^4+2p^2l^2\cos 2\phi}, \qquad (29)$$

where the following function

$$\Psi(p_1,\phi,\phi_1) = \left[l\cos\phi_1 + L\sin(\phi+\phi_1)\right]\times \ln\frac{L^2+R^2+l^2+2LR\cos(\phi+\phi_1)+2Ll\sin\phi-2Rl\sin\phi_1}{L^2+p_1^2+l^2+2Lp_1\cos(\phi+\phi_1)+2Ll\sin\phi-2xl\sin\phi_1} - l\cos\phi_1\ln\frac{R^2+l^2-2Rl\sin\phi_1}{p_1^2+l^2-2p_1l\sin\phi_1} \qquad (30)$$

is introduced. Here l denotes the distance between the GB dislocations which compose the ragged dislocation walls with the disclinations at the edges (Fig.24). This distance may be written through the magnitude of the Burgers vector $\vec{B}$ of the GB dislocations and the disclination strength ω as

$$l \approx B/\omega. \qquad (31)$$

In its turn, the Burgers vector $\vec{B}$ is connected with other geometric parameters of this defect configuration by the relations: $B = b_1\cos\phi_1 + b\cos\phi$ and $b_1/b = \sin\phi/\sin\phi_1$. Their substitution into equation (31) gives

$$l \approx \frac{b\sin(\phi+\phi_1)}{\omega\sin\phi_1}. \qquad (32)$$

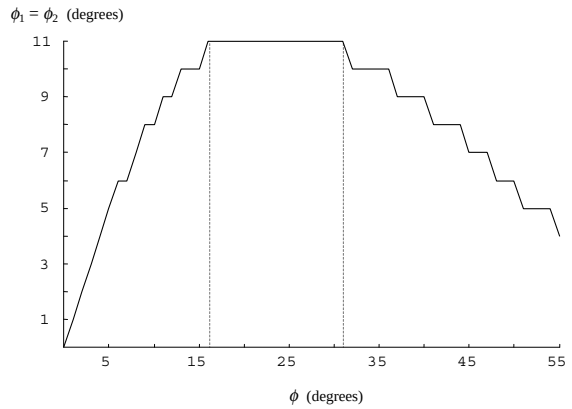

Fig. 25. ϕ-dependence of the angles ϕ_1 and $\phi_2(=\phi_1)$ corresponding to the minimum of the energy difference ΔW, for the following parameters of the model: $\omega=0.1$, $p_1=p_2=p=b$, $\sigma=5\cdot10^{-3}G$, $R=10^7 b$ and $L=1000b$.

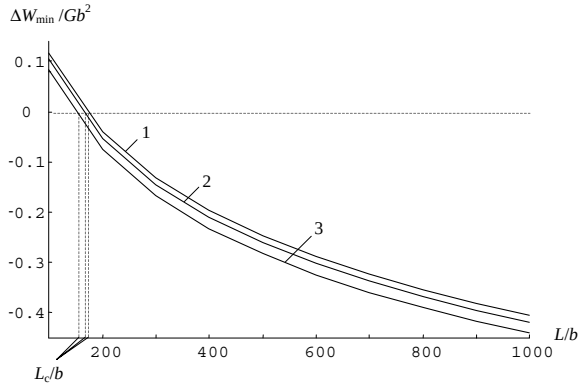

Fig. 26. Dependence of the energy difference ΔW on the disclination dipole arm L, for the following parameters of the model: $\omega=0.1$, $p_1=p_2=p=b$, $\sigma=5\cdot10^{-3}G$, $R=10^7 b$ and $\phi=30°$ (curve 1), 40° (2) and 50° (3).

The energy of interaction $E^{b_1}_{b_2}$ between the $\vec{b}_1$- and $\vec{b}_2$-dislocations is also calculated as the work spent to generate one dislocation in the stress field of the other. The result is [176]

$$E^{b_1}_{b_2} = -Db_1b_2\left(\frac{S_1S_2}{P^2}+\cos(\phi_1-\phi_2)\ln\frac{R}{|P|}\right), \qquad (33)$$

where the following denotations

$$\begin{aligned} &S_1 = p_1\sin(\phi_1-\phi_2)-L\sin(\phi+\phi_2),\\ &S_2 = p_2\sin(\phi_1-\phi_2)+L\sin(\phi+\phi_1),\\ &P^2 = L^2+p_1^2+p_2^2+2p_1p_2\cos(\phi_1-\phi_2)+\\ &2Lp_1\cos(\phi+\phi_1)+2Lp_2\cos(\phi+\phi_2) \end{aligned} \qquad (34)$$

are used.

The energy of interaction $E^{b_i}_{bb}$ of the $\vec{b}_i$-dislocation with the dipole of $\pm\vec{b}$-dislocations is determined in a similar way that results in [176]

$$E^{b_i}_{bb} = \frac{Dbb_i}{2}\Phi(p_i,\phi,\phi_i), \qquad (35)$$

where i=1, 2 and

$$\begin{aligned} &\Phi(p_i,\phi,\phi_i) = \cos(\phi+\phi_i)\\ &\times\ln\frac{(L-p)^2+p_i^2+2(L-p)p_i\cos(\phi+\phi_i)}{p^2+p_i^2+2pp_i\cos(\phi+\phi_i)}-\\ &\frac{2p_i(L-2p)(p^2+p_i^2-Lp)\sin^2(\phi+\phi_i)}{\left[(L-p)^2+p_i^2+2(L-p)p_i\cos(\phi+\phi_i)\right]\left[p^2+p_i^2+2pp_i\cos(\phi+\phi_i)\right]} \end{aligned} \qquad (36)$$

The energies of interaction of the lattice dislocations with the external stress σ are given by simple formulae

$$E^{b_i}_{\sigma} = -\frac{\sigma}{2}b_ip_i\sin2\phi_i, \qquad (37)$$

$$E^{b}_{\sigma} = -\frac{\sigma}{2}bp\sin2\phi. \qquad (38)$$

Thus, all terms of sums (24) and (25) are obtained. The energy difference $\Delta W=W_2-W_1$ may then be written in the following final form [176]:

$$\begin{aligned} \Delta W = &\frac{D}{2}\left\{\left(b_1^2+b_2^2\right)\left(\ln\frac{R}{r_c}+1\right)+\right.\\ &2b^2\left(\ln\frac{|L-2p-r_c|}{r_c}+1\right)\\ &-2b_1b_2\left(\frac{S_1S_2}{P^2}+\cos(\phi_1-\phi_2)\ln\frac{R}{|P|}\right)-\\ &\frac{\sigma}{D}\left(2bp\sin2\phi+b_1p_1\sin2\phi_1+b_2p_2\sin2\phi_2\right)+\\ &b\left[b_1\Phi(p_1,\phi,\phi_1)+b_2\Phi(p_2,\phi,\phi_2)\right]+\\ &\omega\left[b_1\Psi(p_1,\phi,\phi_1)+b_2\Psi(p_2,-\phi,-\phi_2)\right]-\\ &\left.\omega bl\cos\phi\ln\frac{(L-p)^4+l^4+2(L-p)^2l^2\cos2\phi}{p^4+l^4+2p^2l^2\cos2\phi}\right\}. \end{aligned} \qquad (39)$$

The results of numerical calculations carried out by using formula (39) are presented in Figs. 25 and 26 [176, 177]. Thus, the dependences of the characteristic angles ϕ_1 and ϕ_2 on the angle ϕ are shown in Fig.25, in the case with $\phi_1=\phi_2$. These dependences, for the given values of ϕ, indicate the angles ϕ_1 and ϕ_2 at which the disclination dipole motion (Fig.24) is characterized by the lowest value ΔW_{min} (where $\Delta W<0$) of the energy difference (39) that corresponds to the start of the disclination dipole motion. (In other words, ΔW_{min} is the largest energy gain due to the start of motion of emitted lattice dislocations, associated with the process in question). As it follows from Fig.25, these angles ϕ_1 and $\phi_2(=\phi_1)$ increase with rising ϕ from 0° to ≈15°, have the constant value of ≈11° in the range of ϕ from ≈15° to ≈30°, and decrease from ≈11° to ≈4° with rising ϕ from ≈30° to ≈55°.

The angles ϕ_1 and $\phi_2(=\phi_1)$, which correspond to the minimum of the energy difference ΔW, depend weakly on other parameters L, σ, and ω of the system. At the same time, the minimum value ΔW_{min} of this characteristic energy difference is sensitive to the parameters discussed. In Fig. 26, the dependences of ΔW_{min} on the disclination dipole arm L are presented for various values of the angle ϕ [177]. It follows from Fig. 26 that the disclination dipole motion is energetically favourable ($\Delta W_{min}<0$) if the dipole arm L exceeds a critical value L_c, which is ϕ dependent and close to about $150b \approx 50$ nm. In the range of ϕ from 1° to tentatively 30°, the dependences $\Delta W_{min}(L)$ coincide; they are presented as curve 1 in Fig. 26. The dependences $\Delta W_{min}(L)$ at ϕ=40° and 50° (see curves 2 and 3 respectively in Fig.26) are different from those at $\phi \leq 30°$. They indicate that $\Delta W_{min}(L)$ slightly decreases with rising ϕ from 30° to 50°. To summarize, $\Delta W_{min}<0$, that is the disclination dipole motion (Fig.24) is an energetically favourable process within rather wide ranges of parameters that characterize the defect configuration under consideration.

Thus, in papers [176, 177], it has been theoretically revealed that the rotational mode of plastic flow in the fine-grained materials produced by severe plastic deformation can effectively occur via the GB disclination dipole motion associated with the emission of lattice dislocation pairs into the adjacent grains (Fig.24). In contrast to the previously considered [8, 156] situation with the disclination motion associated with the absorption (ordered in space and time) of lattice dislocations by GBs, the disclination dipole motion associated with the emission of lattice dislocation pairs does not require any correlated flux of dislocations from grain interiors to GBs. This micromechanism for the disclination motion can be responsible for the rotations of grains experimentally observed [152-156, 168-173] in the fine-grained materials under (super)plastic deformation and thermal treatment.

3.3. Crossover from grain boundary sliding to rotational deformation

In the previous Sections we have considered the motion of partial disclinations which is realized by absorption (Section 2) or emission (Sections 3.1 and 3.2) of lattice dislocations. Thus, cooperative action of the translational (dislocation gliding) and rotational (disclination motion) modes of plastic deformation in NCMs has been assumed. However, as we have already mentioned above, with grain refinement below a critical grain size d^* the gliding of lattice dislocations stops to play any significant role in NCMs, and new micromechanisms of plasticity as GB sliding and diffusion mass transfer are activated. The question arises how the rotational mode of plasticity can develop in these conditions. In the present Section we discuss the results of recent theoretical investigation of relation between the micromechanisms of GB sliding and diffusion, and rotational deformation which occurs through generation and motion of partial GB disclinations by means of the climb of GB dislocations along GBs in NCMs [184]. It is demonstrated that under special conditions of plastic deformation, the crossover from the translational micromechanism of plasticity (GB sliding) to the rotational one (grain rotation) is possible.

3.3.1. Splitting of gliding grain boundary dislocations at triple junction into climbing dislocations (small-scale view)

GB sliding which is treated to be the dominant mode of superplasticity in nano- and microcrystalline materials occurs via motion of gliding GB dislocations. They have Burgers vectors that are parallel with corresponding GB planes along which these dislocations glide. Triple junctions of GBs, where GB planes change their orientations, serve as obstacles for the GB dislocation motion. In these circumstances, splitting of gliding GB dislocations can occur at triple junctions, resulting in the formation of sessile dislocations and gliding dislocations providing the further GB sliding along the adjacent GBs [185]. However, in general, GB dislocations stopped at a triple junction are also capable of being split into climbing GB dislocations (Fig.27) [184]. When this process repeatedly occurs at a triple junction, it results in the formation of two walls of GB dislo-

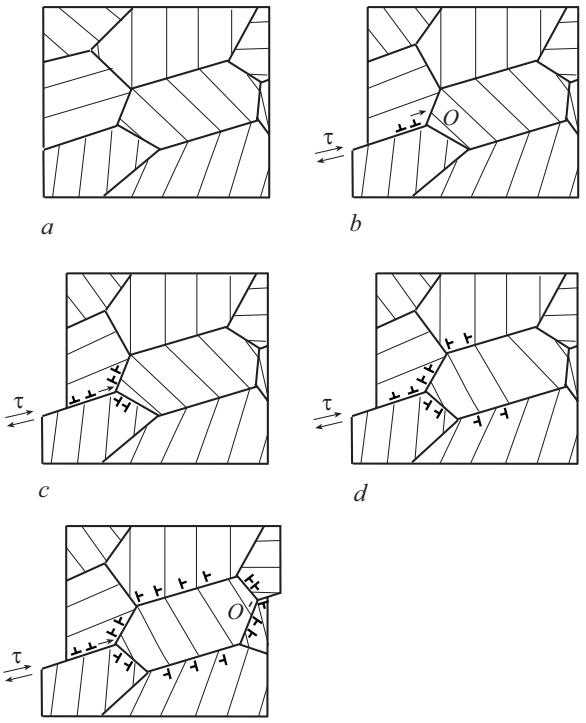

Fig. 27. Combined action of grain boundary sliding and rotational deformation mode. (a) Nanocrystalline specimen in a non-deformed state. (b) Grain boundary sliding occurs via motion of gliding grain boundary dislocations under shear stress action. (c) Gliding dislocations split at triple junction *O* of grain boundaries into climbing dislocations. (d) The splitting of gliding grain boundary dislocations repeatedly occurs causing the formation of walls of grain boundary dislocations whose climb is accompanied by crystal lattice rotation in a grain. (e) Climbing dislocations reach triple junction *O'* where they converge into gliding dislocations causing further grain boundary sliding.

cations climbing along the GBs adjacent to the triple junction. The climbing GB dislocation walls cause the rotational deformation, in which case the repeatedly occurring splitting of gliding GB dislocations at the triple junction provides the crossover from the GB sliding to the rotational deformation mode. This process can be spread over the grain which has to rotate on an angle as a whole. Thus, the stopped GB sliding can stimulate plastic rotation of the neighbour grain. Obviously this mechanism may only be effective under the condition of intensive GB diffusion of vacancies which must be capable to provide the necessary velocity of GB dislocation climb.

The reality of the model [184] may be estimated from the viewpoint of thermodynamics (by analysing the energetic favoritism of this process and obtaining only the necessary conditions of its realization) or kinetics (which allows to find its sufficient conditions). In the framework of the first approach, which has already been demonstrated many times through this review, the problem is solved relatively simply and gives new results (see below). The second approach means the necessity to state and solve a very complicated problem of GB diffusion for vacancies in a system with many sources and sinks, with account for highly inhomogeneous field of elastic stresses of the dislocation-disclination structure that evolves in space and time. Such a problem have neither been stated nor solved yet. Using the first approach, the authors [184] have considered the very beginning of the transition from the GB sliding to the formation of final disclination structure, when the "head" GB dislocation in a pile-up splits into a

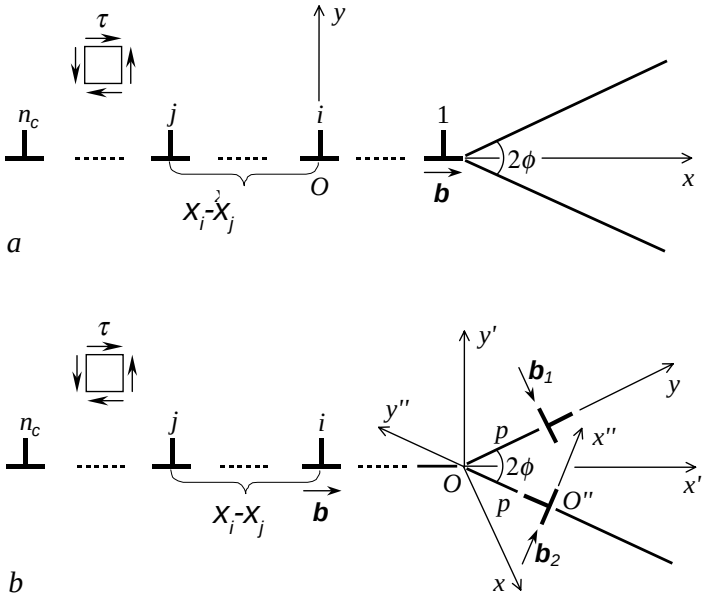

Fig. 28. Splitting of the (a) head dislocation of a grain boundary dislocation pile-up at a triple junction into (b) two dislocations that climb along the adjacent grain boundaries. Coordinate systems *Oxy*, *Ox'y'* and *O"x"y"* are shown which have been used in calculations.

pair of new GB dislocations (small-scale view; see the current Section 3.3.1), and the very end of this transition, when two pile-ups of GB dislocations at the opposite sides of a grain are totally transformed into a system of GB disclination dipoles (large-scale view; see Section 3.3.2).

Following the model [184], consider a pile-up of n_c GB dislocations having the Burgers vectors $\vec{b}$ near a triple junction of GBs under the action of external shear stress τ (Fig.28a). Assume that the head GB dislocation splits into the two new GB dislocations with Burgers vectors $\vec{b}_1$ and $\vec{b}_2$, which can climb along the adjacent GBs (Fig.28b). The splitting process may be characterized by the difference $\Delta W=W_2-W_1$ between the energies of the final (W_2, Fig.28b) and initial (W_1, Fig.28a) states of the defect configuration. The splitting is energetically favorable (unfavorable), if $\Delta W<0$ ($\Delta W>0$, respectively). The equation $\Delta W=0$ gives a set of critical values of parameters for the defect configuration, at which the splitting becomes energetically favorable.

The total energy W_1 of the initial defect configuration (per unit dislocation length) consists of two terms [184]

$$W_1 = E_1^{pu} + E_{\Sigma 1}^{b-b}, \tag{40}$$

where E_1^{pu} is the sum of the self energies of n_c GB dislocations composing the pile-up, and $E_{\Sigma 1}^{b-b}$ is the energy that characterizes pair interactions between all these dislocations.

The first term is written at once as [141]

$$E_1^{pu} = n_c \frac{Db^2}{2}\left(\ln\frac{R}{b}+1\right). \tag{41}$$

In order to find the second term, let us first calculate the energy $E_{ij}^{b\text{-}b}$ that characterizes elastic interaction between the *i*th and *j*th GB dislocations of the pile-up, with the distance $(x_i\text{-}x_j)$ between them (Fig.28a). The positions x_i and x_j of these dislocations may be calculated [186] with the help of the Laguerre polynomials $L_n(x)$ which are determined as solutions of the differential equation

$$x^2\frac{d^2y}{dx^2}+(1-x)\frac{dy}{dx}+ny=0. \tag{42}$$

The first derivative of the Laguerre polynomial $L'_n(x)$ is a solution of the equation

$$x\frac{d^2y}{dx^2}+(2-x)\frac{dy}{dx}+(n-1)y=0 \tag{43}$$

and is given by the following formula

$$L_n'(x) = -\sum_{k=0}^{n-1}\frac{n!(-x)^k}{k!(k+1)!(n-k-1)!}. \tag{44}$$

Eshelby et al. [186] showed that the roots of the first derivative of the Laguerre polynomial $L'_n(x)$ determine the equilibrium positions of dislocations in a discrete dislocation pile-up. Thus, by calculating numerically the positions of the GB dislocations in the pile-up for the given values of n_c and τ (Fig.28a), one can also find the energy of elastic interaction between two GB dislocations as the work spent to transfer one dislocation from a free surface of a solid to its current position in the stress field created by the other dislocation. A similar approach has been used for analysing dislocation interactions within a GB dislocation pile-up in work [185]. In doing so, the energy $E_{ij}^{b\text{-}b}$ of interaction between the *i*-th and *j*-th GB dislocations has been found as [184]

$$E_{ij}^{b-b} = Db^2\ln\frac{R}{x_i-x_j}. \tag{45}$$

The energy $E_{\Sigma 1}^{b-b}$ that characterizes pair interactions between all GB dislocations belonging to the pile-up (Fig.28a) is the sum of energies $E_{ij}^{b\text{-}b}$ over the GB dislocation indices *i* and *j* ($i \neq j$) [184]:

$$E_{\Sigma 1}^{b-b} = \sum_{i=1}^{n_c-1}\sum_{j=i+1}^{n_c}E_{ij}^{b-b} = Db^2\sum_{i=1}^{n_c-1}\sum_{j=i+1}^{n_c}\ln\frac{R}{x_i-x_j}. \tag{46}$$

The energy of the defect configuration (Fig.28b) resulted from the splitting of the head dislocation belonging to the GB dislocation pile-up consists of nine terms [184]:

$$W_2 = E_2^{pu} + E_{\Sigma 2}^{b-b} + E_s^{b_1} + E_s^{b_2} + E_{\Sigma 2}^{b-b_1} + E_{\Sigma 2}^{b-b_2} + E^{b_1-b_2} + E^{\tau-b_1} + E^{\tau-b_2}, \tag{47}$$

where E_2^{pu} is the sum of all self energies of the GB dislocations belonging to the pile-up after the splitting, $E_{\Sigma 2}^{b-b}$ the energy of pair interactions between all GB dislocations composing the pile-up, $E_s^{b_1}$ and $E_s^{b_2}$ are the self energies of the two GB dislocations resulted from the splitting of the head dislocation, $E_{\Sigma 2}^{b-b_1}$ and $E_{\Sigma 2}^{b-b_2}$ are the energies that characterize interaction between GB dislocations of the pile-up and the GB dislocations resulted from the splitting and characterized by Burgers vectors $\vec{b}_1$ and $\vec{b}_2$, respectively; $E^{b_1-b_2}$ is the energy of interaction between these latter (climbing) dislocations; and $E^{\tau-b_1}$ and $E^{\tau-b_2}$ are the effective works of the shear

stress τ, spent to transfer these two GB dislocations along the GBs adjacent to the triple junction.

The pile-up after the splitting of its head dislocation (Fig.28b) contains (n_c-1) GB dislocations. To simplify the calculations of the energy characteristics of these dislocations, the authors [184] have assumed that the dislocation positions remain unchanged during the splitting of the head dislocation. This assumption is reasonable in at least the situation where the GB dislocations resulted from the splitting are close to the triple junction (Fig.28b). Then the first term of the sum (47), E_2^{pu}, is directly obtained from formula (41) through replacement of n_c by (n_c-1). The second term, $E_{\Sigma 2}^{b-b}$, yields from formula (46) with substitution of i=1 for i=2 in the lower limit of the first sum.

The self energies of the new climbing GB dislocations, $E_s^{b_1}$ and $E_s^{b_2}$, are well known [141]. They are given by the r.h.s. of equation (19) with replacement of the cut-off radius r by b_1 and b_2, respectively.

Calculation of the energies of interaction between the GB dislocations of the pile-up and the climbing GB dislocations has been carried out in the following way [184]. First, the energy of interaction between the climbing dislocation and an arbitrary dislocation of the pile-up has been found. This procedure is quite cumbersome because it includes the determination of the shear stress created by the climbing dislocation, which acts in the plane of the pile-up, with further calculation of the work spent to generate a dislocation from the pile-up in this shear stress field. For example, the energy of interaction of the b_1-dislocation with the i-th dislocation from the pile-up has been obtained as [184]

$$E_i^{b-b_1} = Dbb_1 \sin\phi\left(\frac{p^2 + Rp\cos\phi}{R^2 + 2Rp\cos\phi + p^2} - \frac{p^2 + x_i p\cos\phi}{x_i^2 + 2x_i p\cos\phi + p^2} + \frac{1}{2}\ln\frac{R^2 + 2Rp\cos\phi + p^2}{x_i^2 + 2x_i p\cos\phi + p^2}\right), \quad (48)$$

where 2ϕ is the angle between the GBs along which the $\vec{b}_1$- and $\vec{b}_2$-dislocations climb, p the path of the $\vec{b}_1$-dislocation, and x_i the coordinate of the i-th dislocation in the pile-up (Fig.28b). In a similar way, the energy $E_i^{b\text{-}b2}$ of interaction of the $\vec{b}_2$-dislocation with the i-th dislocation in the pile-up is calculated. Therefore, the total energy that charactrizes interaction of both the $\vec{b}_1$- and $\vec{b}_2$-dislocations with GB dislocations of the pile-up reads [184]

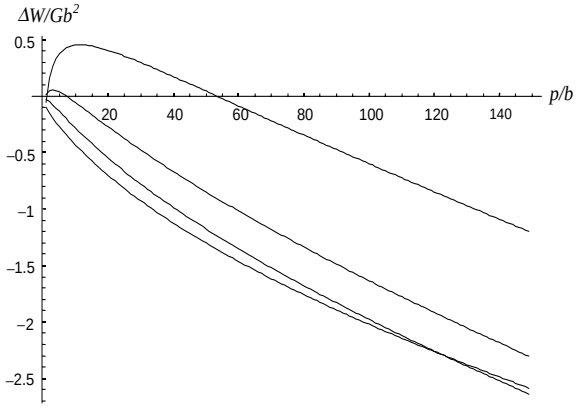

Fig. 29. Dependences of ΔW (in units of Gb^2) on distance p (in units of b) moved by climbing $\vec{b}_1$- and $\vec{b}_2$-dislocations, for 2ϕ =40, 60, 80 and 120° (from top to bottom).

$$E_{\Sigma 2}^{b-b_1} + E_{\Sigma 2}^{b-b_2} = \sum_{i=1}^{n_c}\left(E_i^{b-b_1} + E_i^{b-b_2}\right). \quad (49)$$

The energy $E^{b_1-b_2}$ of interaction between the climbing dislocations is also calculated as the work on generation of one dislocation in the stress field of the other. Omitting intermediate results, we give the final formula [184]:

$$E^{b_1-b_2} = -\frac{Db_1b_2}{2}\left(\frac{2R^2}{R^2\,\mathrm{cosec}^2\phi - 4Rp\,\mathrm{ctg}\phi + 4p^2} + \cos 2\phi \ln\frac{R^2 - 2Rp\sin 2\phi + 4p^2\sin^2\phi}{4p^2\sin^2\phi}\right). \quad (50)$$

The work $E^{\tau-b_k}$ spent to transfer the $\vec{b}_k$-dislocation by distance p under the shear stress τ is equal to

$$E^{\tau-b_k} = -b_k p\tau\sin 2\phi. \quad (51)$$

Thus, we have all terms figuring in the energy difference ΔW=W_2-W_1 that characterizes the splitting (Fig.28) considering as an elementary act of the crossover from the GB sliding to the rotational deformation mode in NCMs. The numerical results for the dependences $\Delta W(p)$, which have been obtained for b_1=b_2=b/(2sinϕ), n_c=5, R=$10^7 b$, τ=G/200 and different values of the angle 2ϕ, are presented in Fig.29 [184]. These curves show that the splitting - an elementary act of the crossover from the GB sliding to the rotational mode – is energetically favorable at large values (80°-120°) of the angle 2ϕ.

In paper [185] it has been demonstrated that the splitting of the head GB dislocation of a pile-up stopped at a triple junction into two, gliding and sessile, GB dislocations is energetically favorable at low values of the angle 2ϕ. That version of the splitting serves as an elementary act of the GB sliding at triple junctions.

Thus, the crossover from the GB sliding to the rotational deformation (Figs.27 and 28) occurs effectively at triple junctions with large values of the angle 2ϕ, while the GB sliding itself occurs effectively at triple junctions with comparatively low values of the angle 2ϕ.

3.3.2. Cooperative action of grain boundary sliding and rotational deformation mode in nanocrystalline materials (large-scale view)

Consider, how the system of defects described in the previous Section can develop in time under an external shear stress [184]. After the head GB dislocation has split into the $\vec{b}_1$- and $\vec{b}_2$-dislocations (Fig.28b), their stress fields prevent movement of the second GB dislocation of the pile-up towards the triple junction where the splitting has occurred. When the climbing $\vec{b}_1$- and $\vec{b}_2$-dislocations move far from the triple junction, their effect on the second GB dislocation of the pile-up becomes weak. In this case the second dislocation of the pile-up moves to the triple junction where it splits into two GB dislocations climbing along the adjacent GBs. Such a splitting process repeatedly occurs transforming GB dislocations of the pile-up into the climbing GB dislocations (Fig.27). These climbing dislocations form dislocation walls of finite extent at the two GBs adjacent to the triple junction. The geometric and elastic properties of these two ragged dislocation walls are similar to those of the corresponding two-axes dipoles of partial wedge disclinations [8, 133] (see also Sections 2 and 3.1).

Now assume that similar splitting processes occur at two opposite triple junctions of GBs surrounding a nano-sized grain. The GB dislocation pile-ups located near the opposite triple junctions consist of dislocations with the Burgers vectors of opposite signs, which tend to move under the shear stress action towards each other and are stopped by the triple junctions. Such a pile-up consisting of n_c dislocations in its initial state may be represented effectively as a superdislocation with the Burgers vector $\pm\vec{B}=\pm n_c\vec{b}$ (Fig.30a). Following the model [184], these two superdislocations split and are transformed into four GB dislocation walls of finite extent, which are effectively represented as four dipoles of disclinations (Fig.30b).

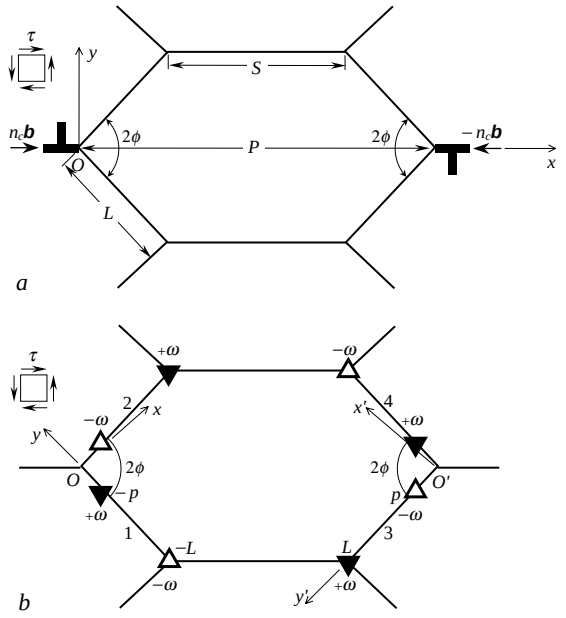

Fig. 30. Large-scale model of crossover from grain boundary sliding to rotational deformation mode. (a) Two superdislocations (models of pile-ups of grain boundary dislocations) are stopped at the opposite triple junctions. (b) Four disclination dipoles (models of climbing dislocation walls) are located at the grain boundaries adjacent to the triple junctions.

In calculating the energy characteristics of evolution of the GB dislocation ensemble, causing grain rotation, for definiteness and simplicity, the authors [184] have made the following model assumptions: (i) The grain is a hexagon with the angles 2ϕ characterizing the splitting processes at the opposite triple junctions being the same. (ii) Magnitudes of the Burgers vectors of all GB dislocations belonging to the dislocation pile-ups are the same. (iii) The plane of the shear stress action is parallel with planes of GBs where the GB dislocation pile-ups are located. (iv) All the disclinations modeling the walls of the climbing GB dislocations have the same strength magnitude ω. Also the total number $2n_c$ of GB dislocations participating in the transformations have believed to be constant. It is worth noting that all these assumptions are not necessary and may be omitted in a more general model.

Following the authors [184], consider the conditions which are necessary for realization of the total transformation of two initial pile-ups of GB dislocations (Fig.30a) into four ragged walls of climbing GB dislocations modeled by four dipoles of GB disclinations (Fig.30b). The transformation of the GB dislocation ensemble may be characterized by the

difference $\Delta\tilde{W}=\tilde{W}_2-\tilde{W}_1$ between the energies of the final ($\tilde{W}_2$) and initial ($\tilde{W}_1$) states of the ensemble. The transformation is energetically favorable (unfavorable), if $\Delta\tilde{W}<0$ ($\Delta\tilde{W}>0$, respectively).

In the framework of the model discussed, the energy of the dislocation ensemble in its initial state (Fig.30a) consists of the three terms [184]:

$$\tilde{W}_1 = 2E_1^{pu} + 2E_{\Sigma 1}^{b-b} + E_{\text{int}}^{B-B}, \tag{52}$$

where the two first terms are already known — they describe the sum of self energies of the GB dislocations in the pile-ups ($2E_1^{pu}$) and the sum of all energies of pair interactions between the GB dislocations within their pile-ups ($2E_{\Sigma 1}^{b-b}$). They are determined by formulae (41) and (46), respectively. The third term, E_{int}^{B-B}, is the energy that characterizes pair interactions between GB dislocations belonging to the different pile-ups. In the first approximation, this energy may be estimated as the energy of elastic interaction of two superdislocations with the Burgers vectors $\pm\vec{B}$ [184]:

$$E_{\text{int}}^{B-B} = -DB^2 \ln\frac{R}{P}, \tag{53}$$

where P is the distance between the opposite triple junctions.

Thus, the energy (52) of the system in its initial state is approximated by the sum of three terms. The two first terms strictly take into account the fine structure of the dislocation pile-ups (i.e., the specific distributions of dislocations within the pile-ups), while the third one is approximated by equation (53), which does not account for this fine structure. However, this approximation (when a pile-up is treated as a superdislocation) gives rather good results if the distance P (Fig.30a) is much larger than the pile-up length [141]. The latter must be smaller than $S/2$, and S is assumed to be always smaller (two or more times, see below) than P in the model [184]. Therefore, the pile-up length must be four or more times smaller then P, and the approximation of superdislocations in calculating the term (53) is thus proved.

The energy of the GB dislocation ensemble in its final state (Fig.30b) consists of the six terms [184]:

$$\tilde{W}_2 = 4E_s^{\Delta} + 4E_{\tau}^{\Delta} + 2E_{\tau}^{pu} + 2E_{\text{int}}^{1-2} + 2E_{\text{int}}^{1-3} + 2E_{\text{int}}^{1-4}, \tag{54}$$

where E_s^{Δ} denotes the self-energy of a disclination dipole, E_{τ}^{Δ} the work spent to transfer the GB dislocations resulted from the splitting under the shear stress τ, E_{τ}^{pu} the work spent to transfer all GB dislocations belonging to the pile-ups from their initial positions up to the corresponding triple junctions under the shear stress τ, and E_{int}^{i-j} the energy of interaction between the i-th and j-th disclination dipoles ($i \neq j$; i=1,2,3; j=2,3,4).

The total self energy E_s^{Δ} of the disclination dipole with the arm (L-p) and strength ω is given by formula (17) with replacement of L by (L-p), N by n_c, and b by b_1.

The shear stress τ acts on the climbing GB dislocations which compose the disclination dipoles. The work E_{τ}^{Δ} spent to climb of n_c dislocations within one disclination dipole is [184]

$$E_{\tau}^{\Delta} = -\tau b_1 \sin 2\phi\left(p + \frac{n_c(n_c-1)b_1}{2\omega}\right). \tag{55}$$

This work is the same for all the disclination dipoles under consideration (Fig.30b).

The GB dislocations of each pile-up consequently move under the shear stress τ action from their initial positions $x=x_i$, to the new positions at the triple junctions (x=0). The work E_{τ}^{pu} spent to the transfer of all the GB dislocations of a pile-up is [184]

$$E_{\tau}^{pu} = -\tau b\sum_{i=1}^{n_c}|x_i|. \tag{56}$$

The energy E_{int}^{i-j} of elastic interaction between the i-th and j-th disclination dipoles is calculated as the work spent to generate one dipole in the stress field of the other. Omitting cumbersome intermediate calculations, we give the final results [184]:

$$E_{\text{int}}^{1-2} = \frac{D\omega^2}{4}\left\{\Psi_-(x',L,0,0,y',\phi) - \Psi_-(x',p,0,0,y',\phi)\right\}\Big|_{x'=0}^{x'=R}\Big|_{y'=p}^{y'=L}, \tag{57}$$

$$E_{\text{int}}^{1-3} = \frac{D\omega^2}{4}\left\{\Psi_+(x',L,T,T',y',\phi) - \Psi_+(x',p,T,T',y',\phi)\right\}\Big|_{x'=0}^{x'=R}\Big|_{y'=p}^{y'=L}, \tag{58}$$

$$E_{\text{int}}^{1-4} = \frac{D\omega^2}{4}\left\{\Psi_+(x',T',T,L,y',0) - \Psi_+(x',T',T,p,y',0)\right\}\Big|_{x'=0}^{x'=R}\Big|_{y'=p}^{y'=L}, \tag{59}$$

where,

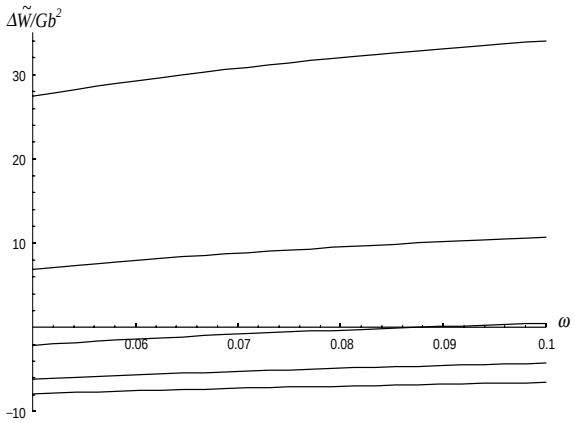

Fig. 31. Dependences of $\Delta\tilde{W}$ (in units of Gb^2) on disclination strength ω in the range of values of the triple junction angle 2ϕ =60, 80, 100, 120 and 160° (from top to bottom).

$$\Psi_{\pm}(x',l,t,t',y',\phi) = \left\{(x'+t)^2 + l^2 + (y'-t')^2 \pm 2l(y'-t')\cos 2\phi \mp 2l(x'+t)\sin 2\phi\right\} \times \ln\left\{(x'+t)^2 + l^2 + (y'-t)^2 \pm 2l(y'-t')\cos 2\phi \mp 2l(x'+t)\sin 2\phi\right\} \quad (60)$$

and $T=P\sin\phi$, $T'=P\cos 2\phi$.

Thus, all terms figuring in formulae (52) for the energy $\tilde{W}_1$ and (54) for the energy $\tilde{W}_2$, which compose the characteristic difference $\Delta\tilde{W}=\tilde{W}_2-\tilde{W}_1$, have been found. If $\Delta\tilde{W}$ is negative (positive), the transformation of the defect configuration is energetically favorable (unfavorable, respectively). The authors [184] have analysed numerically the dependence of $\Delta\tilde{W}$ on the disclination dipole strength ω (Fig.31). The calculations have been carried out for $b_1=b_2=b/(2\sin\phi)$, n_c=5, $R=10^7b$, $\tau=G/200$, $L=200b$, $P=400b$ and different values of the angle 2ϕ that characterizes geometry of the triple junction. The plots $\Delta\tilde{W}(\omega)$ show that the transformation is most favorable in the range of 2ϕ from 100° to 160°. Also, the magnitude of $\Delta\tilde{W}$ (that is, the energy gain due to the transformation when $\Delta\tilde{W}<0$) decreases with an increase of the disclination strength ω (ranging from 0.05 to 0.1).

3.3.3. Critical stress of crossover from grain boundary sliding to rotational deformation

The equation $\Delta\tilde{W}=0$ allows one to calculate the critical shear stress τ_c at which the crossover from GB sliding to rotational deformation (Fig.30) occurs. This equation may be written as follows [184]:

$$\tau_c = \frac{\tilde{W}_2' - \tilde{W}_1(\tau_c)}{2b\sum_{i=1}^{n_c}|x_i(\tau_c)| + 4b_1\sin 2\phi\left\{p + \frac{n_c(n_c-1)b_1}{2\omega}\right\}}, \quad (61)$$

where $\tilde{W}_2'$ is given by formula (54) for $\tilde{W}_2$ with terms $4E_\tau^\Delta$ and $2E_\tau^{pu}$ removed.

Let us consider how τ_c changes depending on the values of the angle 2ϕ and grain size P. The authors [184] have used the following characteristic values of parameters of a NCM and defect configuration under consideration. The Poisson ratio ν has been equal to 0.3. Moduli of the GB dislocation Burgers vectors and disclination strength have been taken as follows: b=0.1 nm and ω=0.1 (≈5.7°). The number n_c has been varied from 3 to 20 together with the distance L to keep the disclination strength ω constant. The distance p has also been assumed to be constant and equal to l. These assumptions are considered reasonable based on the information available. As we will see later, actual form of the curves is not too sensitive on the values.

Now express the distance L through S and P, whose ratio $q=S/P<1$. Then we have [184]

$$L = \frac{1-q}{2\cos\phi}P. \quad (62)$$

With formulas under discussion, for the above characteristic values of parameters, the dependences of the critical shear stress τ_c on the grain size (diameter) P have been calculated in [184]. These dependences are shown for q=0.5 (Fig.32a) and q=0.1 (Fig.32b), for different values of the triple junction angle 2ϕ. The curves $\tau_c(P)$ lie, in general, in different ranges of P because the disclination strength ω is taken constant here. Therefore, increase in P leads to increase in both L and n_c, and this relation depends on the angle 2ϕ. For the sake of convenience, the points corresponding to n_c = 3 (triangles), 5 (pentagons) and 15 (circles) are attached to every curve. The upper ends of the curves correspond to n_c=20. As a result, one can additionally trace how τ_c depends on the angle 2ϕ when both the L and n_c keep constant.

From Fig.32 it follows that τ_c decreases with the decrease of P (grain refinement) [184]. This is the main result of this section. It demonstrates that the smaller grains are rotated easier (they are rotated

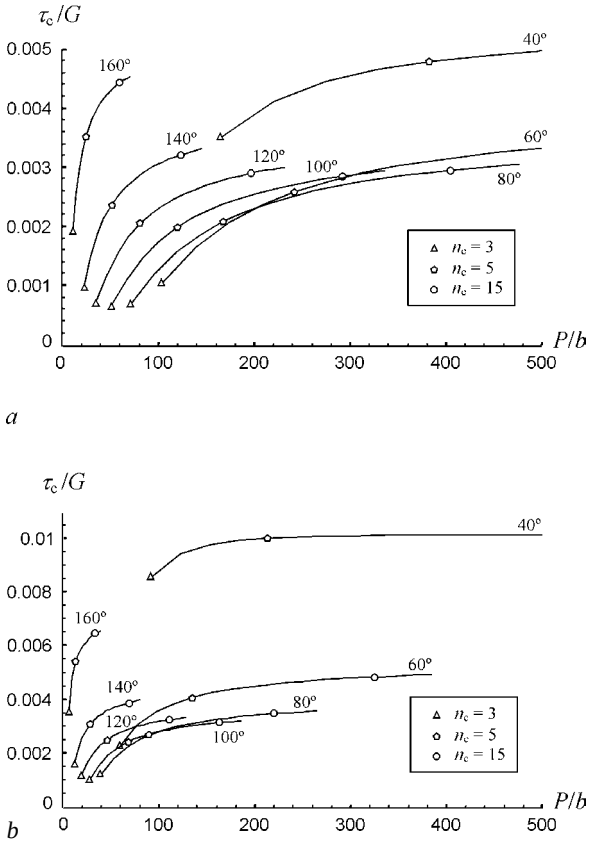

Fig. 32. Dependence of the critical shear stress τ_c on the grain size P, (a) for q=0.5 and (b) for q=0.1, for different values of the triple junction angle 2ϕ given by figures at the curves. The numbers of grain boundary dislocations n_c are shown by the triangles (n_c=3), pentagons (n_c=5) and circles (n_c=15).

under the action of smaller critical stress τ_c) than the larger ones. Moreover, τ_c strongly depends on the grain shape (i.e., on q and 2ϕ). Increase in q leads to decrease in τ_c because larger q (for the fixed values of P and 2ϕ) needs smaller number n_c of GB dislocations to spread along the GB (or smaller dipole arm L-p). The dependence of τ_c on the angle 2ϕ is more complicated. For the fixed L and n_c, in the range of relatively small angles, $2\phi < 100°$, the critical stress τ_c decreases with increasing 2ϕ and achieves its minimum at $2\phi \approx 100°$. In the range of relatively large angles, $2\phi > 100°$, the critical stress τ_c increases with rising 2ϕ.

Thus, one can conclude that the smaller grains that are characterized by the larger q and $2\phi \approx 100°$, need the smaller critical stress τ_c to rotate [184].

The theoretical models for motion of GB disclinations considered in Section 3 allow us to conclude the following:

- Motion of GB disclinations is an effective mechanism of rotational deformation in NCMs.
- Motion of GB disclinations may be realized through the micromechanisms of emission of lattice dislocations or climb of GB dislocations. Realization of these micromechanisms are possible in wide ranges of values of the main geometry and force parameters of the system.
- Motion of GB disclinations by means of lattice dislocation emission is effective until the usual dislocation plasticity is possible in nanograins. When the glide of lattice dislocations is replaced by the GB sliding, appearance of GB dislocation pile-ups at the GB triple junctions and further transformation of these pile-ups into the walls of climbing GB dislocations (the dipoles of GB disclinations) serve as a possible way to activate the rotational mode of plastic deformation in NCMs.
- The transition from the GB sliding to the rotational deformation becomes energetically favorable when the external shear stress achieves its critical value which depends on the elastic properties of the NCM, structure of its GBs, grain size and shape. The smaller grains need the smaller critical stress to rotate.

4. GENERAL CONCLUSIONS

The rotational mode of plastic deformation in NCMs occurs through nucleation and development of specific (rotational) defect structures which consist of lattice and/or GB dislocations and may be described effectively by means of partial disclinations. Rotational structures are generated in NCMs at various imperfections of GBs (kinks, double and triple junctions, etc.) where the misorientation angle sharply changes. Development of rotational plasticity depends on the mechanisms of translational plasticity which dominate in the given NCM. Domination of lattice gliding may result in appearance of misorientation bands (or other disclination structures which are typical for conventional metals and alloys, but have not been considered here) inside the grains or motion of GB disclinations through emission of lattice dislocations. Domination of GB sliding may lead to formation and motion of GB disclinations through climb of GB dislocations. In both the latter cases, the motion of GB disclinations along their GBs changes the misorientation of crystalline lattices across the GBs and may serve as a mechanism of grain rotation in the process of external mechanical loading.

ACKNOWLEDGEMENTS

This work was supported, in part, by the Office of US Naval Research (grant N00014-01-1-1020), the Russian Fund of Basic Research (grant 01-02-16853), Russian State Research Program on Solid-State Nanostructures, RAS Program "Structural Mechanics of Materials and Constructions", St.Petersburg Scientific Center, and "Integration" Program (grant B0026).

REFERENCES

[1]. R. Birringer and H. Gleiter, In: *Advances in Materials Science, Encyclopedia of Materials Science and Engineering*, v. 1, ed. by R.W.Cahn (Pergamon Press, Oxford, 1988), p. 339.

[2]. H. Gleiter // *Progr. Mater. Sci.* **33** (1989) 223.

[3]. V.G. Gryaznov, A.M. Kaprelov and A.E. Romanov, In: *Disclinations and Rotational Deformation of Solids*, ed. by V.I.Vladimirov (Ioffe Physico-Technical Institute, Leningrad, 1988), p. 47, in Russian.

[4]. V.G. Gryaznov, A.M. Kaprelov, I.A. Polonskii and A.E. Romanov // *Phys. Stat. Sol. (b)* **167** (1991) 29.

[5]. V.G. Gryaznov, A.M. Kaprelov, A.E. Romanov and I.A. Polonskii // *Phys. Stat. Sol. (b)* **167** (1991) 441.

[6]. I.A. Polonsky, A.E. Romanov, V.G. Gryaznov and A.M. Kaprelov // *Phil. Mag. A* **64** (1991) 281.

[7]. L.I. Trusov, M.Yu. Tanakov, V.G. Gryaznov, A.M. Kaprelov and A.E. Romanov // *J. Cryst. Growth* **114** (1991) 133.

[8]. A.E. Romanov and V.I. Vladimirov, In: *Dislocations in Solids*, v. 9, ed. by F.R.N.Nabarro (North-Holland, Amsterdam, 1992), p. 191.

[9] V.G. Gryaznov and L.I. Trusov // *Progr. Mater. Sci.* **37** (1993) 290.

[10]. A.E. Romanov, I.A. Polonsky, V.G. Gryaznov, S.A. Nepijko, T. Junghaus, N.I. Vitrykhovski // *J. Cryst. Growth* **129** (1993) 691.

[11]. A.E. Romanov, In: *Nanostructured Materials: Science and Technology,* ed. by G.-M.Chow and N.I.Noskova (Kluwer Academic Publishers, Dordrecht/Boston/London, 1998), p. 207.

[12]. M.Yu. Gutkin and I.A. Ovid'ko // *Nanostruct. Maters.* **2** (1993) 631.

[13]. M.Yu. Gutkin and I.A. Ovid'ko, In: *Strength of Materials*, ed. by H.Oikawa, K.Maruyama, S.Takeuchi and M.Yamaguchi (The Japan Institute of Metals, Sendai, 1994), p. 227.

[14]. D.A. Konstantinidis and E.C. Aifantis // *Nanostruct. Maters*. **10** (1998) 1111.

[15]. S.G. Zaichenko and A.M. Glezer // *Phys. Solid State* **39** (1997) 1810.

[16]. M.Yu. Gutkin, I.A. Ovid'ko and C.S. Pande // *Rev. Adv. Mater. Sci.* **2** (2001) 80.

[17]. M.Yu. Gutkin, I.A. Ovid'ko and C.S. Pande, In: *Nanoclusters and Nanocrystals, Ch. 8*, ed. by H.S.Nalwa (American Scientific Publishers, 2003).

[18]. G. Palumbo, U. Erb and K.T. Aust // *Scr. Metall. Mater.* **24** (1990) 2347.

[19]. A.V. Osipov and I.A. Ovid'ko // *Appl. Phys. A* **54** (1992) 517.

[20] M.Yu. Gutkin and I.A. Ovid'ko // *Phil. Mag. A* **70** (1994) 561.

[21] M.Yu. Gutkin, K.N. Mikaelyan and I.A. Ovid'ko // *Phys. Solid State* **37** (1995) 300.

[22] M.Yu. Gutkin, I.A. Ovid'ko and K.N. Mikaelyan // *Nanostruct. Maters.* **6** (1995) 779.

[23] A.A. Nazarov, A.E. Romanov and R.Z. Valiev // *Nanostruct. Maters*. **6** (1995) 775.

[24] M.Yu. Gutkin, K.N. Mikaelyan and I.A. Ovid'ko // *Phys. Stat. Sol. (a)* **153** (1996) 337.

[25] A.A. Nazarov, A.E. Romanov and R.Z. Valiev // *Scr. Mater*. **34** (1996) 729.

[26] P. Müllner and W.-M. Kuschke // *Scr. Mater.* **36** (1997) 1451.

[27] R.Z. Valiev and I.V. Alexandrov, *Nanostructured Materials Obtained by Intensive Plastic Deformation* (Logos, Moscow, 2000), in Russian.

[28] F.K. LeGoues, M. Copel and R. Tromp // *Phys. Rev. Lett.* **63** (1989) 1826.

[29] F.K. LeGoues, M. Copel and R. Tromp // *Phys. Rev. B* **42** (1990) 11690.

[30] C.S. Ozkan, W.D. Nix and H. Gao // *Mater. Res. Soc. Proc.* **399** (1996) 407.

[31] C.S. Ozkan, W.D. Nix and H. Gao // *Appl. Phys. Lett.* **70** (1997) 2247.

[32] P. Müllner, H. Gao and C.S. Ozkan // *Phil. Mag. A* **75** (1997) 925.

[33] H. Gao, C.S. Ozkan, W.D. Nix, J.A. Zimmerman and L.B. Freund // *Phil. Mag. A* **79** (1999) 349.

[34] I.A. Ovid'ko // *J. Phys.: Condens. Matter* **11** (1999) 6521.

[35] I.A. Ovid'ko // *Phys. Solid State* **41** (1999) 1500.

[36] A.G. Sheinerman and M.Yu. Gutkin // *Phys. Stat. Sol. (a)* **184** (2001) 485.
[37] A.L. Kolesnikova, A.E. Romanov and I.A. Ovid'ko // *Solid State Phenomena* **87** (2002) 265.
[38] I.A. Ovid'ko, A.G. Sheinerman and N.V. Skiba // *J. Phys.: Condens. Matter* **15** (2003) 1173.
[39] A.E. Romanov, In: *Experimental Investigation and Theoretical Description of Disclinations*, ed. by V.I.Vladimirov (Ioffe Physico-Technical Institute, Leningrad, 1984), p. 110, in Russian.
[40] A.E. Romanov // *Mater. Sci. Eng. A* **164** (1993) 58.
[41] M.Yu. Gutkin, A.L. Kolesnikova and A.E. Romanov // *Mater. Sci. Eng. A* **164** (1993) 433.
[42] A.L. Kolesnikova, In: *Experimental Investigation and Theoretical Description of Disclinations*, ed. by V.I.Vladimirov (Ioffe Physico-Technical Institute, Leningrad, 1984), p. 194, in Russian.
[43] A.L. Kolesnikova, N.D. Priemskii and A.E. Romanov, *Preprint No. 869,* (Ioffe Physico-Technical Institute, Leningrad, 1984), in Russian.
[44] V.I. Vladimirov, A.L. Kolesnikova and A.E. Romanov // *Phys. Metals Metallogr.* **60** (1985) 58.
[45] A.L. Kolesnikova and A.E. Romanov, *Preprint No. 1019* (Ioffe Physico-Technical Institute, Leningrad, 1986), in Russian.
[46] A.G. Zembilgotov and N.A. Pertsev, In: *Disclinations and Rotational Deformation of Solids*, ed. by V.I.Vladimirov (Ioffe Physico-Technical Institute, Leningrad, 1988), p. 158, in Russian.
[47] A.Yu. Belov // *Phil. Mag. Letters* **64** (1991) 207.
[48] A.Yu. Belov // *Phil. Mag. A* **65** (1992) 1429.
[49] A.L. Kolesnikova and A.E. Romanov // *Phys. Solid State* **45** (2003) 1626.
[50] Y.Z. Povstenko // *Int. J. Engng. Sci.* **33** (1995) 575.
[51] Y.Z. Povstenko // *J. Physique IV* **8** (1998) 309.
[52] M.Yu. Gutkin and E.C. Aifantis // *Phys. Stat. Sol. (b)* **214** (1999) 245.
[53] M.Yu. Gutkin and E.C. Aifantis // *Phys. Solid State* **41** (1999) 1980.
[54] M.Yu. Gutkin and E.C. Aifantis, In: *Nanostructured Films and Coatings, NATO ARW Series, High Technology*, v. 78, ed. by G.-M.Chow, I.A.Ovid'ko and Y.Tsakalakos (Kluwer, Dordrecht, 2000), p. 247.
[55] M.Yu. Gutkin // *Rev. Adv. Mater. Sci*. **1** (2000) 27.
[56] M. Lazar // *Phys. Lett. A* **311** (2003) 416.
[57] M. Lazar // *J. Phys.: Condens. Matter* (2003), in press.
[58] H. Gleiter // *Phys.* **47** (1991) 753.
[59] H. Gleiter // *Nanostruct. Mater.* **1** (1992) 1.
[60] U. Erb, A.M. El-Sherik, G. Palumbo and K.T. Aust // *Nanostruct. Mater.* **2** (1993) 383.
[61] R.W. Siegel // *Mater. Sci. Eng. A* **168** (1993) 189.
[62] R.W. Siegel // *Nanostruct. Mater.* **4** (1994) 121.
[63] N.I. Noskova, In: *Contemporary Problems of Physics and Mechanics of Materials* (Saint-Petersburg State University, Saint-Petersburg, 1997), p. 333, in Russian.
[64] A.I. Gusev // *Physics-Uspekhi* **41** (1998) 49.
[65] R.A. Andrievskii and A.M. Glezer // *Phys. Metals Metallogr.* **88** (1999) 45.
[66] R.A. Andrievskii and A.M. Glezer // *Phys. Metals Metallogr*. **89** (2000) 83.
[67] H. Gleiter // *Acta Mater.* **48** (2000) 1.
[68] I.A. Ovid'ko // *Rev. Adv. Mater. Sci*. **1** (2000) 61.
[69] R.A. Andrievskii // *Perspektivnye Materialy* No. **6** (2001) 5, in Russian.
[70] R.A. Andrievski // *Mater. Trans.* **42** (2001) 801.
[71] R.A. Andrievski and G.V. Kalinnikov // *Surf. Coat. Technology* **142-144** (2001) 573.
[72] J. Eckert, A. Reger-Leonhard, B. Weiss, M. Heilmaier and L. Schultz // *Adv. Eng. Mater*. **3** (2001) 41.
[73] D.V. Shtanskii and E.A. Levashov // *Izvestiya VUZov. Tsvetnaya Metallurgiya* No. **3** (2001) 52, in Russian.
[74] I.A. Ovid'ko, In: *Science and Technology of Interfaces, International Symposium in Honor of Dr. Bhakta Rath*, ed. by S. Ankem, C.S. Pande, I. Ovid'ko and S. Ranganathan (TMS, Warrendale, 2002), p. 245.
[75] I.A. Ovid'ko, In: *Encyclopedia of Nanoscience and Nanotechnology*, Chapter 4, ed. by H.S.Nalwa (American Sci. Publ., California, 2003).
[76] V.M. Fedosyuk, *Multilayered Magnetic Structures* (Belorussian State University, Minsk, 2000), in Russian.

[77] A.I. Gusev and A.A. Rempel, *Nanocrystalline Materials* (Nauka, Moscow, 2000), in Russian.
[78] M.Yu. Gutkin and I.A. Ovid'ko, *Defects and Mechanisms of Plasticity in Nanostructured and Non-crystalline Materials* (Yanus, Saint-Petersburg, 2001), in Russian.
[79] Yu.R. Kolobov, R.Z. Valiev, G.P. Grabovetskaya, A.P. Zhilyaev, E.F. Dudarev, K.V. Ivanov, M.B. Ivanov, O.A. Kashin and E.B. Naidenkin, *Grain-Boundary Diffusion and Properties of Nanostructured Materials* (Nauka, Novosibirsk, 2001), in Russian.
[80] V.M. Fedosyuk and T.A. Tochitskii, *Electrolitically deposited nanostructures* (Belorussian State University, Minsk, 2002), in Russian.
[81] *Proceedings of the Second International Conference on Nanostructured Materials* (Stuttgart, Germany, October 3-7, 1994), ed. by H.-E.Schaefer, R.Würschum, H.Gleiter and T.Tsakalakos // *Nanostruct. Mater.* **6** (1995) 533.
[82] *Nanomaterials: Synthesis, Properties and Application*s, ed. by A.S.Edelstain and R.C.Cammarata (Institute of Physics Publ., Bristol and Philadelphia, 1996).
[83] *Structure, Phase Transformations and Properties of Nanocrystalline Alloys* (Ural Department of Russian Academy of Sciences, Ekaterinburg, 1997), in Russian.
[84] *R&D Status and Trends in Nanoparticles, Nanostructured Materials, and Nanodevices in the United States,* ed. by R.W.Siegel, E.Hwu and M.C.Roco (International Technology Research Institute, Baltimore, 1997).
[85] *Nanostructured Materials: Science and Technology,* ed. by G.-M.Chow and N.I.Noskova (Kluwer Academic Publishers, Dordrecht/Boston/London, 1998).
[86] *Handbook of Nanostructured Materials and Nanotechnology,* Vols. 1-5, ed. by H.S.Nalwa (Academic Press, San Diego, 1999).
[87] *Material Science of Carbides, Nitrides and Borides*, ed. by Y.G.Gogotsi and R.A.Andrievski (Kluwer Academic Publishers, Dordrecht/Boston/London, 1999).
[88] *Mechanical Behavior of Nanostructured Materials* // *MRS Bulletin* **24** (1999) 14.
[89] *Nanostructured Films and Coatings,* NATO ARW Series, High Technology, v. **78,** ed. by G.-M.Chow, I.A.Ovid'ko and T.Tsakalakos (Kluwer, Dordrecht, 2000).
[90] *Structure and Mechanical Properties of Nanophase Materials - Theory and Computer Simulations vs. Experiment,* ed by D.Farkas, H.Kung, M.Mayo, J.Van Swygenhoven and J.Weertman (MRS, Warrendale, 2001).
[91] *Problems of Nanocrystalline Materials*, ed. by V.V.Ustinov and N.I.Noskova (Ural Department of Russian Academy of Sciences, Ekaterinburg, 2002), in Russian.
[92] *Nanophase and Nanocomposite Materials IV, MRS Symp. Proc*., v. **703**, ed. by S.Komarneni, R.A.Vaia, G.Q.Lu, J.- I.Matsushita and J.C.Parker (MRS, Warrendale, 2003).
[93] *Nanomaterials for Structural Applications, MRS Symp. Proc.,* v. **740**, ed. by C.C.Berndt, T.Fischer, I.A.Ovid'ko, G.Skandan and T.Tsakalakos (MRS, Warrendale, 2003).
[94] U. Herr, J. Jing, R. Birringer, U. Conser and H. Gleiter // *Appl. Phys. Lett.* **50** (1987) 472.
[95] H.-E. Schaefer and R. Würshum // *Phys. Lett. A* **119** (1987) 370.
[96] R. Würshum, M. Scheytt and H.-E. Schaefer // *Phys. Stat. Sol. (a)* **102** (1987) 119.
[97] X. Zhu, R. Birringer, U. Herr and H. Gleiter // *Phys. Rev. B* **35** (1987) 9085.
[98] T. Haubold, R. Birringer, B. Lengeler and H. Gleiter // *Phys. Lett. A* **135** (1989) 461.
[99] E. Jorra, H. Franz, J. Peisl, G. Wallner, W. Petry, T. Haubold, R. Birringer and H. Gleiter // *Phil. Mag. B* **60** (1989) 159.
[100] W. Wunderlich, Y. Ishida and R. Maurer // *Scr. Metall. Mater.* **24** (1990) 403.
[101] A.H. King // *Interf. Sci.* **7** (1999) 251.
[102] V.B. Rabukhin // *Poverkhnost'. Fizika, Khimiya, Mekhanika* No. **7** (1986) 126, in Russian.
[103] G. Palumbo and K.T. Aust // *Mater. Sci. Eng. A* **113** (1989) 139.
[104] K.M. Yin, A.H. King, T.E. Hsieh, F.R. Chen, J.J. Kai and L. Chang // *Microscopy and Microanalysis* **3** (1997) 417.
[105] U. Czubayko, V.G. Sursaeva, G. Gottstein and L.S. Shvindlerman, In: Grain Growth in Polycrystalline Materials III, ed. by H.Weiland, B.L.Adams and A.D.Rollett (TMS, Pittsburg, 1998), p. 423.
[106] G. Gottstein, A.H. King and L.S. Shvindlerman // *Acta Mater.* **48** (2000) 397.
[107] K. Owusu-Boahen and A.H. King // *Acta Mater.* **49** (2001) 237.
[108] A.A. Fedorov, M.Yu. Gutkin and I.A. Ovid'ko // *Scr. Mater.* **47** (2002) 51.

[109] J. Horvath, R. Birringer and H. Gleiter // *Solid State Comm.* **62** (1987) 319.
[110] H.-E. Schaefer, R. Würschum, T. Gessmann, G. Stöckl, P. Scharwaechter, W. Frank, R.Z. Valiev, H.-J. Fecht and C. Moelle // *Nanostruct. Mater.* **6** (1995) 869.
[111] Yu.R. Kolobov, G.P. Grabovetskaya, I.V. Ratochka and K.V. Ivanov // *Nanostruct. Mater.* **12** (1999) 1127.
[112] Yu.R. Kolobov, G.P. Grabovetskaya, K.V. Ivanov, R.Z. Valiev and T.C. Lowe, In: *Investigations and Applications of Severe Plastic Deformation,* NATO Science Ser., ed. by T.C.Lowe and R.Z.Valiev (Kluwer, Dordrecht, 2000), p. 261.
[113] V.V. Rybin, *Large Plastic Deformations and Fracture of Metals* (Metallurgia, Moscow, 1986), in Russian.
[114] M. Seefeldt // *Rev. Adv. Mater. Sci.* **2** (2001) 44.
[115] P. Klimanek, V. Klemm, A.E. Romanov and M. Seefeldt // *Adv. Eng. Maters.* **3** (2001) 877.
[116] Local Lattice Rotations and Disclinations in Microstructures of Distorted Crystalline Materials, ed. by P. Klimanek, A.E. Romanov, M. Seefeldt // *Solid State Phenomena* **87** (2002).
[117] U. Essmann // *Phys. stat. sol.* **3** (1963) 932.
[118] I.W. Steeds // *Proc. Roy. Soc. A* **292** (1966) 343.
[119] A.N. Vergazov, V.A. Likhachev and V.V. Rybin // *Fiz. Met. Metalloved.* **42** (1976) 146, in Russian.
[120] G.V. Berezhkova and P.P. Perstnev // *Sov. Phys.-Doklady* **24** (1979) 799.
[121] G.V. Berezhkova, P.P. Perstnev, A.E. Romanov and V.I. Vladimirov // *Cryst. Res. Techn.* **18** (1983) 139.
[122] E.V. Nesterova and V.V. Rybin // *Fiz. Met. Metalloved.* **59** (1985) 395, in Russian.
[123] A.D. Korotaev, A.N. Tyumentsev and V.F. Sukhovarov, *Dispersion Hardening of Refractory Metals* (Nauka, Novosibirsk, 1989), in Russian.
[124] A.D. Korotaev, A.N. Tyumentsev and Yu.P. Pinjin // *Phys. Mesomechanics* **1** (1998) 23.
[125] M.Yu. Gutkin, K.N. Mikaelyan, A.E. Romanov and P. Klimanek // *Phys. Stat. Sol. (a)* **193** (2002) 35.
[126] M. Murayama, J.M. Howe, H. Hidaka and S. Takaki // *Science* **295** (2002) 2433.
[127] V.I. Vladimirov and A.E. Romanov // *Sov. Phys. - Solid State* **20** (1978) 1795.
[128] B.K. Barakhtin, S.A. Ivanov, I.A. Ovid'ko, A.E. Romanov and V.I. Vladimirov // *J. Phys. D* **22** (1989) 519.
[129] A.E. Romanov and E.C. Aifantis // *Scr. Metall. Mater*. **29** (1993) 707.
[130] M. Seefeldt and P. Klimanek // *Mater. Sci. Eng. A* **234-236** (1997) 758.
[131] M. Seefeldt and P. Klimanek // *Model. Simul. Mater. Sci. Eng.* **6** (1998) 349.
[132] K.N. Mikaelyan, M. Seefeldt, M.Yu. Gutkin, P. Klimanek and A.E. Romanov // *Phys. Solid State* **45** (2003) 000.
[133] R. de Wit // *J. Res. Nat. Bur. Stand. A* **77** (1973) 607.
[134] A. Needleman // *Acta mater.* **48 (**2000) 105.
[135] B. Devincre, L.P. Kubin, C. Lemarchand and R. Madec // *Mater. Sci. Eng. A* 3**09-310** (2001) 211.
[136] L. Nicola, E. Van der Giessen and A. Needleman // *Mater. Sci. Eng. A* **309-310** (2001) 274.
[137] N. Argaman, O. Levy and G. Makov // *Mater. Sci. Eng. A* **309-310** (2001) 386.
[138] O. Politano and J.M. Salazar // *Mater. Sci. Eng. A* **309-310** (2001) 261.
[139] H. Yasin, H.M. Zbib and M.A. Khaleel // *Mater. Sci. Eng. A* **309-310** (2001) 294.
[140] P. Rodriguez, D. Sundararaman, R. Divakar and V.S. Raghunathan // *Chem. Sustainable Development* **8** (2000) 69.
[141] J.P. Hirth and J. Lothe, *Theory of Dislocations* (John Wiley, New York, 1982).
[142] M.F. Ashby // *Phil. Mag.* **21** (1970) 399.
[143] U.F. Kocks, A.S. Argon and M.F. Ashby // *Progr. Maters. Sci.* **19** (1975) 1.
[144] K.M. Jassby and T. Vreeland, Jr. // *Phil. Mag.* **21** (1970) 1147.
[145] H. Gleiter // *Mater. Sci. Eng. A* **52** (1982) 91.
[146] A.P. Sutton and R.W. Balluffi, Interfaces in Crystalline Materials (Clarendon Press, Oxford, 1995).
[147] J.P. Hirth // *Acta. Mater.* **48** (2000) 93.
[148] L.G. Kornelyuk, A.Yu. Lozovoi and I.M. Razumovskii // *Philos. Mag. A* **77** (1998) 465.
[149] M.Yu. Gutkin and I.A. Ovid'ko // *Phys. Rev. B* **63** (2001) 064515.
[150] I.A. Ovid'ko, In: *Nanostructured Films and Coatings, NATO ARW Series*, *High Technology,* v. 78, ed. by G.-M.Chow, I.A.Ovid'ko

and T.Tsakalakos (Kluwer, Dordrecht, 2000), p. 231.
[151] S.V. Bobylev, I.A. Ovid'ko and A.G. Sheinerman // *Phys. Rev. B* **64** (2001) 224507.
[152] K.A. Padmanabhan and G.J. Davies, *Superplasticity* (Springer, Berlin, 1980).
[153] J. Pilling and N. Ridle, *Superplasticity in Crystalline Solids* (The Institute of Metals, London, 1989).
[154] O.A. Kaibyshev and F.Z. Utyashev, *Superplasticity, Structure Refinement and Treatment of Hard-Deforming Alloys* (Nauka, Moscow, 2002), in Russian.
[155] M.G. Zelin and A.K. Mukherjee // *Mater. Sci. Eng. A* **208** (1996) 210.
[156] R.Z. Valiev and T.G. Langdon // *Acta Metall.* **41** (1993) 949.
[157] M. Mayo, D.C. Hague and D.-J. Chen // *Mater. Sci. Eng. A* **166** (1993) 145.
[158] M. Jain and T. Christman // *Acta Metall. Mater*. **42** (1994) 1901.
[159] R.S. Mishra, R.Z. Valiev and A.K. Mukherjee // *Nanostruct. Maters.* **9** (1997) 473.
[160] V.V. Astanin, O.A. Kaibyshev and S.N. Faizova // *Scr. Metall. Mater.* **25** (1991) 2663.
[161] H.S. Yang and M.G. Zelin // *Scr. Metall. Mater.* **26** (1992) 1707.
[162] M. Seefeldt and P. Van Houtte // *Mater. Phys. Mech.* **1** (2000) 133.
[163] M.J. Mayo // *Nanostruct. Mater*. **9** (1997) 717.
[164] B. Baudelet // *Scr. Metall. Mater.* **27** (1992) 745.
[165] M.G. Zelin, R.Z. Valiev, M.V. Grabski, J.W. Wyrzykowski, H.S. Yang and A.K. Mukherjee // *Mater. Sci. Eng. A* **160** (1993) 215.
[166] M.G. Zelin and A.K. Mukherjee // *Acta Metall. Mater.* **43** (1995) 2359.
[167] M.G. Zelin and A.K. Mukherjee // *J. Mater. Res.* **10** (1995) 864.
[168] M. Ke, W.W. Milligan, S.A. Hackney, J.E. Carsley and E.C. Aifantis // *Mat. Res. Soc. Symp. Proc.* **308** (1993) 565.
[169] M. Ke, S.A. Hackney, W.W. Milligan and E.C. Aifantis // *Nanostruct. Maters.* **5** (1995) 689.
[170] N.I. Noskova and E.G. Volkova // *Fizika Metallov i Metallovedenie* **91** (2001) 100, in Russian.
[171] N.I. Noskova and E.G. Volkova // *Fizika Metallov i Metallovedenie* **92** (2001) 107, in Russian.
[172] N.I. Noskova, In: *Problems of Nanocrystalline Materials*, ed. by V.V.Ustinov and N.I.Noskova (Ural Department of Russian Academy of Sciences, Ekaterinburg, 2002), p. 159, in Russian.
[173] K.E. Harris, V.V. Singh and A.H. King // *Acta Mater.* **46** (1998) 2623.
[174] K.N. Mikaelyan, I.A. Ovid'ko, and A.E. Romanov // *Mater. Sci. Eng. A* **288** (2000) 61.
[175] I.A. Ovid'ko // *Science* **295** (2002) 2386.
[176] M.Yu. Gutkin, A.L. Kolesnikova, I.A. Ovid'ko and N.V. Skiba // *J. Metastable & Nanostruct.Maters* **12** (2002) 47.
[177] M.Yu. Gutkin, A.L. Kolesnikova, I.A. Ovid'ko and N.V. Skiba // *Phil. Mag. Letters* **82** (2002) 651.
[178] M.Yu. Gutkin, I.A. Ovid'ko and N.V. Skiba // *Techn. Phys. Lett.* **28** (2002) 437.
[179] M.Yu. Gutkin, I.A. Ovid'ko and N.V. Skiba // *Mater. Sci. Eng. A* **339** (2003) 73.
[180] H. Grimmer, W. Bollmann and D.H. Warrington // *Acta Crystall. A* **30** (1974) 197.
[181] M.Yu. Gutkin, K.N. Mikaelyan and I.A. Ovid'ko // *Phys. Solid State* **37** (1995) 300.
[182] M.Yu. Gutkin, I.A. Ovid'ko and K.N. Mikaelyan // *Nanostruct. Maters.* **6** (1995) 779.
[183] M.Yu. Gutkin, K.N. Mikaelyan and I.A. Ovid'ko // *Phys. Stat. Sol. (a)* **153** (1996) 337.
[184] M.Yu. Gutkin, I.A. Ovid'ko and N.V. Skiba // *Acta Mater.* **51** (2003) 4059
[185] A.A. Fedorov, M.Yu. Gutkin and I.A. Ovid'ko // *Acta Mater.* **51** (2003) 887.
[186] J.D. Eshelby, F.C. Frank, and F.R.N. Nabarro // *Phil. Mag.* **42** (1951) 351.